energies

MDPI

Review

Impact of Coolant Operation on Performance and Heterogeneities in Large Proton Exchange Membrane Fuel Cells: A Review

Marine Cornet [1], Erwan Tardy [1,2], Jean-Philippe Poirot-Crouvezier [1] and Yann Bultel [2,*]

[1] Univ. Grenoble Alpes, CEA, LITEN, 38000 Grenoble, France; marine.cornet@univ-grenoble-alpes.fr (M.C.); erwan.tardy@grenoble-inp.fr (E.T.); jean-philippe.poirot@cea.fr (J.-P.P.-C.)
[2] Univ. Grenoble Alpes, Univ. Savoie Mont Blanc, CNRS, Grenoble INP, LEPMI, 38000 Grenoble, France
* Correspondence: yann.bultel@grenoble-inp.fr

Abstract: PEMFCs' operation entails the presence of heterogeneities in the generation of current, heat and water along the active surface area. Indeed, PEMFCs are open systems, and as such, operating heterogeneities are inherent to their operation. A review of the literature reveals numerous attempts to achieve uniform current density distribution. These attempts are primarily focused on bipolar plate design and operating conditions, with the underlying assumption that uniform current density correlates with enhanced performance. Most studies focus on the influence of gas flow-field design and inlet hydrogen and air flow conditioning, and less attention has been paid to the coolant operating condition. However, uncontrolled temperature distribution over a large cell active surface area can lead to performance loss and localized degradations. On this latter point, we notice that studies to date have been confined to a narrow range of operating conditions. It appears that complementary durability studies are needed in order to obtain in-depth analyses of the coupled influence of temperature distribution and gas humidification in large PEMFCs.

Keywords: proton exchange membrane fuel cells; coolant operation; flow-field design; thermal management; performance; heterogeneities

Academic Editor: JongHoon Kim

Received: 27 November 2024
Revised: 20 December 2024
Accepted: 24 December 2024
Published: 30 December 2024

Citation: Cornet, M.; Tardy, E.; Poirot-Crouvezier, J.-P.; Bultel, Y. Impact of Coolant Operation on Performance and Heterogeneities in Large Proton Exchange Membrane Fuel Cells: A Review. *Energies* **2025**, *18*, 111. https://doi.org/10.3390/en18010111

1. Introduction

In the transport sector, which alone accounts for almost 30% of greenhouse gas emissions, the use of hydrogen in vehicles could halve well-to-wheel emissions compared with petrol. Hydrogen energy offers immense potential for advancing the clean energy transition and serves as a powerful solution for achieving widespread and deep decarbonization across sectors like transportation, industry, and construction. Water electrolysis for hydrogen production is not only a method of generating hydrogen energy but also helps mitigate the challenges of intermittency and variability associated with renewable energy sources. It enables the use of surplus energy from solar and wind power by converting electrical energy into chemical energy for storage, thereby improving overall energy efficiency [1,2]. Proton exchange membrane fuel cells (PEMFCs) are a promising technology of hydrogen fuel cells to limit CO_2 emissions for transport applications. They are a particularly attractive option for heavy-duty vehicles [3,4].

It is widely acknowledged that the balance of the plant, in which the PEM fuel cell operates, remains a complex field of study. Many studies have been conducted in order to optimize the feeding, humidification and cooling of reactants to find the most efficient architecture [5–11]. Indeed, the auxiliaries enable the operating conditions for the cell to be set, such as the temperature of the incoming gasses, their relative humidity, their pressure, or the flow rates, which depend on the stoichiometries chosen for the various reactants.

The fuel cell system must therefore be able to control the variables that have an impact on cell voltage, from gas conditioning to cell temperature management. The main function of the cathode fluidic architecture is to control the flow of air entering the fuel cell, its humidification and its pressure. Various solutions have been proposed for humidification by membrane [12–14], by recirculation [9,15–18], or even by injection [19–21]. Extreme simplification of the cathode fluid architecture is only possible by completely eliminating the component needed to humidify the air, thanks to adapted strategies for the design and management of the anode and the cooling circuits [22,23]. For the anode side, the fluidic architecture is able to control the flow and pressure of hydrogen entering the fuel cell, but rarely its humidification. Hydrogen supply can be achieved by different fluid management strategies and different architectures. The simplest architecture consists of supplying hydrogen to the fuel cell in the dead-end anode mode. However, this mode of operation leads to the accumulation of nitrogen at the cell outlet as a result of gas permeation through the membrane [24–26]. Hence, to our knowledge, the most widespread architecture for mobility systems is hydrogen recirculation [27]. In a similar way to air recirculation, water vapour transported through the membrane to the anode is recirculated so as to hydrate the membrane via the anode [5,6,17,28,29]. Some authors highlight the significant impact of humidification on performance [30–37]. Indeed, flooding or drying out may lead to degradation within the membrane–electrode assemblies, particularly on the membrane [35]. The operating conditions recognized as having the greatest influence on fuel cell performance and lifetime are relative humidity (RH) and temperature [38–41].

Finally, the coolant loop allows one to manage the stack/cell temperature and to remove excessive heat from the electrochemical reactions. It is essential for maintaining optimal operating temperatures and ensuring efficient performance. Yakubu et al. [42] provide a comprehensive review of primary cooling techniques and thermal management strategies. The cooling techniques used for PEMFCs are based either on liquid and air cooling or phase change cooling [42,43]. The choice depends on the application of the fuel cell system, inducing different options regarding the heat exchange with the environment. Air cooling is justified for applications where light and small systems are required (small mobile devices, drones, etc.), because the number of auxiliaries dedicated to stack cooling is the lowest. Nevertheless, the heat exchange is generally more efficient in air/liquid heat exchangers, such as radiators commonly used in transport applications. Hence, liquid cooling has been generally used for high power applications, because of its high heat capacity and stability, with the criterion of having a temperature that is as uniform as possible [44]. The temperature of the cell or stack can be regulated in relation to the inlet or outlet temperature of the coolant. Most systems are usually regulated thanks to the coolant outlet to avoid hot spots, as the coolant evacuates heat from its inlet to its outlet. That way, even if the cell or stack generates more heat, the coolant outlet temperature stays constant thanks to the increase in the flow rate. This control strategy also implies a decrease in the coolant flow rate with a constant coolant outlet temperature, inevitably causing a decrease in coolant inlet temperature.

In a PEM fuel cell stack, the operating conditions of the cells are inherently non-homogeneous due to the distribution and the progressive consumption of reactant gasses, the evacuation of reaction products, the cooling, and the current collection when large surface areas are used [45,46]. The local operating conditions are therefore very different from the inlet ones set by the balance of the plant. Furthermore, the distributions are subject to cross interactions, which makes operating heterogeneities a complex phenomenon to understand. To ensure the performance and durability of a PEMFC stack, the management of the temperature, water content and current distributions at the cell scale is essential [47,48]. Water distribution affects local current density production. Miao et al. [49] found that

increasing the gasses' relative humidity at low current and decreasing the gasses' RH at high current tends to homogenise the current density distribution. Indeed, the quantity of water produced by the electrochemical reaction is considerably lower at low current density compared to high current density. On the contrary, at higher power, the massive accumulation of liquid water due to local high current density may lead to flooding, impeding the gas diffusion and resulting in rapid degradation of cell performance [50].

The design of the gas distribution areas and channels of the bipolar plates (BPs) affects, among other things, the reactant mass transfer, the water management, and the heat transfer in the cell. Research into flow fields is therefore essential for better performance and durability. Zhang et al. [51] review the problems encountered with flow-field designs in PEMFCs regarding heat and mass transfer, uniform distribution of the reactants, water management, pressure drop and manufacturing feasibility. Different studies found that hydrogen and air gas flow channels have an impact on the overall performance of PEMFCs. Miao et al. [49] studied the influence of cathode bipolar plate design on the performance and current density distribution of a 108 cm^2 cathode segmented PEMFC for three different designs, including parallel–serpentine, parallel and dot–parallel flow fields. They found that the dot–parallel flow field results in a more uniform distribution of current density and temperature and they conclude that there is a correlation between current density distribution uniformity and performance.

The flow configuration has an influence on the current density distribution as well. Several studies [52–54] have concluded that a counter-flow configuration (air flowing in the opposite direction as the hydrogen) results in overall better cell performance and the most uniform current density along the flow channels. Finally, Morin et al. [55] also emphasize the impact of the flow configuration on the distribution of liquid water content, which is linked to the current density and temperature distributions. Once again, the best performance is obtained with a gas counter-flow configuration, but here, it is not correlated with the most uniform distribution of current density.

Finally, a significant number of studies, including experimental and numerical investigations, have already been conducted to examine the internal temperature characteristics of PEMFCs at the cell [56–60] and even stack scale [61–63]. A high operating temperature increases catalysts' activity and decreases activation loss but can cause drying of membrane–electrode assemblies, which increases ohmic loss and ultimately decreases output voltage. A low operating temperature can, however, cause water condensation and flooding, which impacts the transport of reactants to the active layer. Concerning temperature distribution, Macedo-Valencia et al. [64] developed a single-phase 3D model of a PEMFC stack of five cells operating in counter-flow configuration. They confirmed that the in-plane temperature of the cell increases from the air inlet towards the air outlet. Indeed, the gasses warm up with the heat from the reactions while passing through the channels. Fuller and Newman [65] concluded that membrane hydration is sensitive to the rate of heat removal and that more generally, thermal considerations have an impact on water management. The results of Yan et al. [66] confirm the trend that temperature has an indirect impact on the performance of PEM fuel cells, with a notable influence on membrane humidity and water transport within the gas diffusion layer and catalyst layer. Nandjou et al. [67] have also identified local cold or hot spots in the temperature distribution in different areas of the cell. Other studies show the critical impact of temperature on water distribution, which affects the performance and durability of PEMFCs [68–70].

The first experimental study on operating heterogeneities dates back to 1998 and shows an uneven distribution of the current density on the surface of a segmented single cell [45]. Since then, new technologies of segmented cells have emerged that facilitate the assessment of local current density and temperature [71]. For instance, current scan sensors

on printed circuit boards have been developed to be inserted between two monopolar plates in the centre of a stack. They can be used not only to map the current density but also the temperature distribution. The S++® measurement card uses embedded resistance temperature detectors for temperature measurement and shunts resistors for the current measurement [72–76]. Toharias et al. [77] have used this device to produce a dataset of current density and temperature mapping of a 50 cm^2 PEMFC with parallel–serpentine channels for different flow configurations. The study of Chevalier et al. [78] also uses a segmented printed circuit board with two straight channels to measure the current density distribution along the channels and even visualize the liquid water. Another example of a segmented cell is the multi-instrumented segmented PEMFC of Maranzana et al. [79] that measures current density and temperature and enables the observation of liquid water in the channels by using transparent poly(methyl methacrylate) as the material for the plates. In this study, every segment (at the cathode) is associated with a Hall effect sensor. The use of Hall sensors for current measurement was first introduced by Wieser et al. [80]. A review of Pérez et al. [81] describes the segmented cell techniques used from 1998 to 2010 that also include a third type of segmented cell using a resistor network. Beyond the study of the current density and temperature, water content distribution can also be analyzed thanks to specific experiments. Indeed, neutron imaging is a powerful tool for the in situ measurement of liquid water content inside a stack [82–86]. The stack is exposed to a neutron beam that will scatter and produce an attenuation image. Basu et al. [87,88] established, thanks to a technique using tunable diode laser absorption spectroscopy, that membrane dehydration usually occurs at the gasses' inlet as the gasses, even humidified, are drier at the inlet than at the outlet. Indeed, they collect water while passing through the cell. Water distribution in a cell is especially hard to investigate and several studies have even attempted to model the results obtained using neutron imaging [85,86] or internal resistance [89] to better understand water management.

Among the factors influencing the performance of PEMFCs, coolant operation has been overlooked in the literature until now, considering that we exclude here the works concerning air cooling, either with a direct air flow through bipolar plates [90,91] or with the addition of phase change in a vapour chamber to enhance temperature uniformity [92,93]. Most studies on liquid cooling are based on numerical approaches and focus on testing different flow field or distribution area designs for the coolant channels to ensure uniform temperature distribution [94–100]. However, most of these studies only look at the temperature distribution at low power density or focus on making the temperature distribution as uniform as possible. A uniform temperature distribution is not achievable as the heat flux caused by the electrochemical reactions varies spatially and the coolant gradually heats up as it circulates through the cell. However, it is true that a totally uncontrolled temperature distribution can lead to the formation of hot spots and improper heat dissipation [101,102], as well as localized degradation of the membrane impeding the performance of the PEMFC [70]. Good management of temperature distribution is therefore essential and is achievable thanks to the coolant circuit.

The previous literature review shows that the current density distribution depends on the local reactant concentration and the water content and, to a lesser extent, the local temperature. Gas distributions in the cell are primarily induced by the design of the flow fields and by the flow configuration. The water management depends on the BPs' design but also on the current load, the gasses' RH, the temperature distribution and the water transport mechanism in the cell. It is worth mentioning that improper hydration of the membrane can cause local drying and too much water can cause flooding, blocking the reactants from the active layer. The temperature distribution does not seem to impact the current density directly but rather impacts the water content of the cell, which greatly

influences the current density distribution. The performance of the cell is therefore affected by all these factors, but there is no clear correlation between the uniformity of the current density and the performance of the cell in the studied literature. Operating heterogeneities are therefore a complex phenomenon influenced by several factors and their coupled effects.

One aspect that emerges from this literature review is the lack of studies on the influence of cooling operation on the operating heterogeneities and performance of PEMFCs, both numerically and experimentally. This paper provides a review of the impact of coolant operation on performance and heterogeneities in large PEMFCs. In the following sections, the influence of the cooling flow-field design is first investigated. The flow configuration is discussed in the second section. Finally, the influence of the coolant operating conditions on cell ageing is examined.

2. Cooling Flow-Field Design

Cooling flow fields (CFFs) have been extensively studied in recent decades with the following objectives: (1) to correctly evacuate excessive heat, (2) to obtain a uniform temperature and current distribution, (3) to minimize the pressure drop to limit the power consumption of the cooling system, and (4) to improve the stack efficiency. Numerous coolant flow fields have been designed, including parallel, serpentine, and dotted patterns for the most common geometries [103,104]. Most of the studies in this area are based on numerical approaches.

2.1. Parallel, Serpentine and Spiral Flow Fields

Chen et al. [105] were among the first to explore the design of cooling flow fields. They investigated the coupled cooling process that occurs between fluid flow and heat transfer in the interaction between the solid plate and the coolant flow. Their research aimed to optimize the cooling design of a fuel cell stack using three-dimensional computational fluid dynamics analysis. They introduced the useful index of uniform temperature (IUT), which quantifies the difference between the local temperature T, and the mean temperature $\overline{T}$, of the cooling plate (Equation (1)). The IUT is a crucial metric regarding the thermal management of a cell and continues to be widely used in many studies.

$$\mathrm{IUT} = \frac{\int_V |T - \overline{T}| dV}{\int_V dV}, \quad \text{where } \overline{T} = \frac{\int_V T dV}{\int_V dV} \tag{1}$$

They evaluated six cooling modes, comprising three serpentine-type modes and three parallel-type modes. Their results indicate that the cooling performance of serpentine-type modes could be superior to that of parallel-type modes, as one of the serpentine-type modes was able to reduce the IUT value to as low as 1 K, resulting in a more uniform temperature profile.

Yu et al. [95] conducted a numerical study on the performance of various multi-pass serpentine flow fields for cooling plates, aiming to enhance heat management. They modelled one conventional serpentine flow field, four multi-path serpentine flow fields, and one conventional spiral flow field. The simulation results showed that the conventional serpentine flow field had the largest temperature gradient and highest temperature among the six configurations, indicating weaker cooling performance. In contrast, the four multi-path serpentine flow fields and the spiral flow field demonstrated improved temperature uniformity and lower maximum temperatures, achieving a 40–60% reduction in the temperature gradient compared to the conventional serpentine flow field.

Atyabi et al. [106] conducted numerical simulations of various flow-field configurations, including straight parallel channels (Case A), straight parallel channels with metal foam (Case B), multi-channel serpentine designs (Case C), innovative serpentine channels

(Case D), and integrated metal foam channels (Case E), for both gas and cooling channels (Figure 1a). These simulations incorporated electrochemical and cooling models while also accounting for thermal and electrical contact resistance between the gas diffusion layer and bipolar plates. Their findings indicated that Case D delivered the most effective cooling performance, as evidenced by lower temperature results (Figure 1b), thanks to its multiple flow passes and extended channel length; however, this configuration resulted in a high pressure drop. Additionally, Case D achieved the highest power density at the cell scale among all configurations tested (Figure 1c). Nonetheless, when pressure drop effects are considered, the net power output of Case D is 6.12% lower than that of Case E. The study ultimately underscores the balance between optimizing thermal performance and maximizing net system power output in PEM systems.

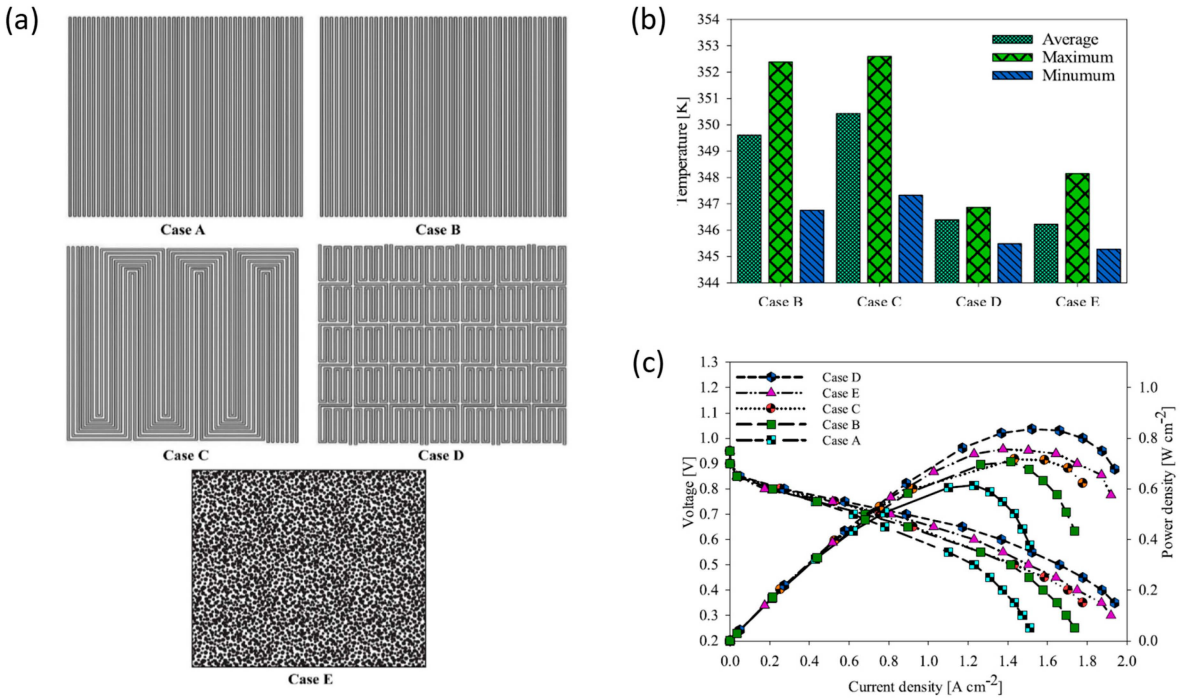

Figure 1. (**a**) Five different cooling flow-field designs: straight parallel channels (case A), straight parallel channels filled with metal foam (Case B), multi-channel serpentine (Case C), novel serpentine channels (Case D) and integrated metal foam (Case E); (**b**) average temperature (membrane), maximum and minimum temperature of the cathode catalyst layer and (**c**) comparison of the polarization curve and power density curves for the various fuel cells [106]. Reproduced with permission from Elsevier.

Recently, Joibary et al. [107] explored the impact of various cooling flow channels on thermal distribution using a 3D large fuel cell model. They designed one parallel flow field and five more complex serpentine flow fields. Their results indicated that the four-section serpentine geometry provided the best temperature uniformity, achieving a lower IUT value compared to the other designs. However, this geometry did not deliver the highest performance or output power among the configurations tested. Zhang et al. [108] studied the effect of channel and rib dimensions of a complicated serpentine-like flow field using a 3D fuel cell model focused on fluid and thermal behaviour. They found a major impact on the pressure drop of the circuit but a minimal effect on the in-plane temperature uniformity.

Finally, Xu et al. [109] introduced a thermal economic index to numerically compare three flow-field designs, considering both the IUT and a quality factor comparing the heat evacuated and the power of the coolant pump. They selected the design with the best

thermal economic index for the realization and study of a 120-cell stack, despite its poor performance in terms of IUT.

In recent years, many studies have focused on improving temperature uniformity in cooling flow fields using conventional serpentine, parallel, and spiral designs [97,110–115]. Their findings align with the previously mentioned studies, showing that while parallel flow channels offer the simplest fabrication process and the lowest pressure drop, they have the poorest cooling performance compared to spiral and serpentine designs.

2.2. Wavy and Oblique Flow Fields

Particularly adapted to stamped metallic bipolar plate, structures featuring wavy and oblique flow fields have been proposed to minimize pressure drop while achieving optimal temperature distribution [23]. In the initial phase of their study, Huo et al. [116] developed a single heat transfer model of a large fuel cell with an active area of 335 cm^2 to analyze the effects of different coolant channel configurations on temperature distribution. They simulated four configurations: both straight channels at the cathode and anode (S + S), straight channels at the cathode and wavy channels at the anode (S + W), and wavy channels at both the anode and cathode with either an identical waveform (SW) or different waveform (DW) (Figure 2a). Their results showed that the S + S configuration yielded the lowest pressure drop (Figure 2b) but led to the greatest heat accumulation among the four configurations. The S + W and DW configurations exhibited less uniform temperature distributions, with heat accumulation occurring at the junctions between the cathode and anode channels, and also had the highest pressure drop, necessitating greater pumping power (Figure 2b). Ultimately, their findings suggest that the SW configuration offers the best balance, providing a fairly uniform temperature distribution with a pressure drop that is only slightly higher than that of the S + S channels (Figure 2b).

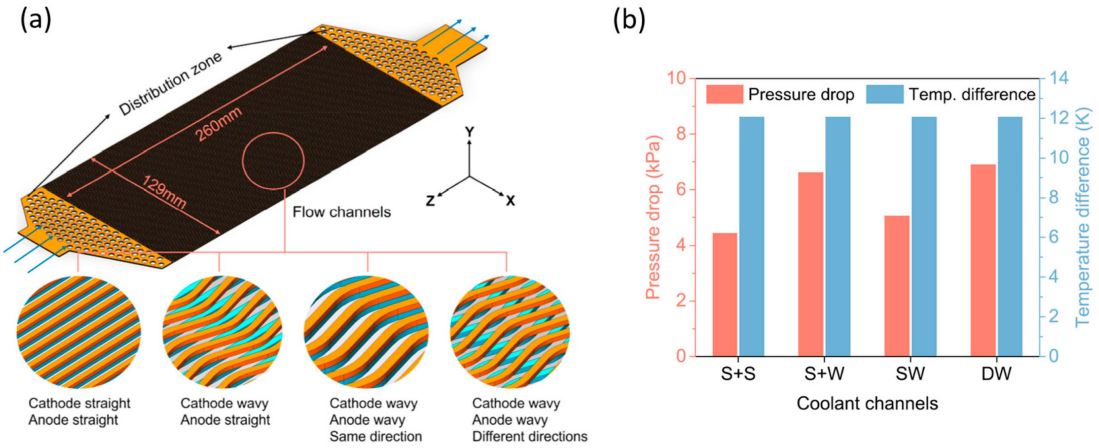

Figure 2. (**a**) Computational domains of four configurations of coolant channel of a large-size proton exchange membrane fuel cell including straight + straight (S + S), straight + wavy (S + W), same waveform (SW) and different waveform (DW) channels and (**b**) pressure drops and temperature differences of the four configurations [116]. Reproduced with permission from Elsevier.

Chen et al. [117] proposed a novel bipolar plate structure featuring a wave-staggered round table cooling flow field. Their numerical results, obtained using a multi-physics and multi-component model, confirm that a wavy CFF provides a better cooling effect compared to a straight CFF. Further, using a three-dimensional multi-phase PEMFC electrochemical model coupled with a cooling channel, Chen et al. [118] demonstrated that the performance of a PEMFC with a wavy CFF is slightly superior to that with a straight CFF.

Sasmito et al. [111] conducted a numerical evaluation of various coolant channel designs, including conventional parallel and serpentine channels, oblique-fin channels, and a hybrid parallel–serpentine–oblique–fin design. Their results showed that serpentine-based channel designs offered superior thermal, water, and gas management, as well as overall stack performance, compared to the other designs. However, the net performance of the conventional serpentine design was lower than that of the oblique–fin channel design, primarily due to its higher pressure drop and parasitic losses. The hybrid parallel–serpentine–oblique–fin channel design proposed in their study provided the best balance between effective thermal management and net power output, thanks to a significantly lower pressure drop. Zhu et al. [119] enhanced a traditional parallel flow field by incorporating tapered oblique fin channels into the ribs to mitigate localized overheating in an air-cooled PEM fuel cell (Figure 3). They conducted a numerical analysis, utilizing a three-dimensional, two-phase model to compare the modified design with the conventional one. Their findings revealed substantial improvements in mass transfer and cell performance at elevated humidity levels (>60%). Additionally, their study indicated that the modified design also leads to improved temperature uniformity. In a follow-up study, Zhu et al. [120] validated their earlier findings through an extended experimental investigation involving a stack of five cells, which included the oblique–fin air-cooled configuration and supplementary simulations. However, they did not address the manufacturing complexities associated with implementing this design on a larger scale compared to traditional designs.

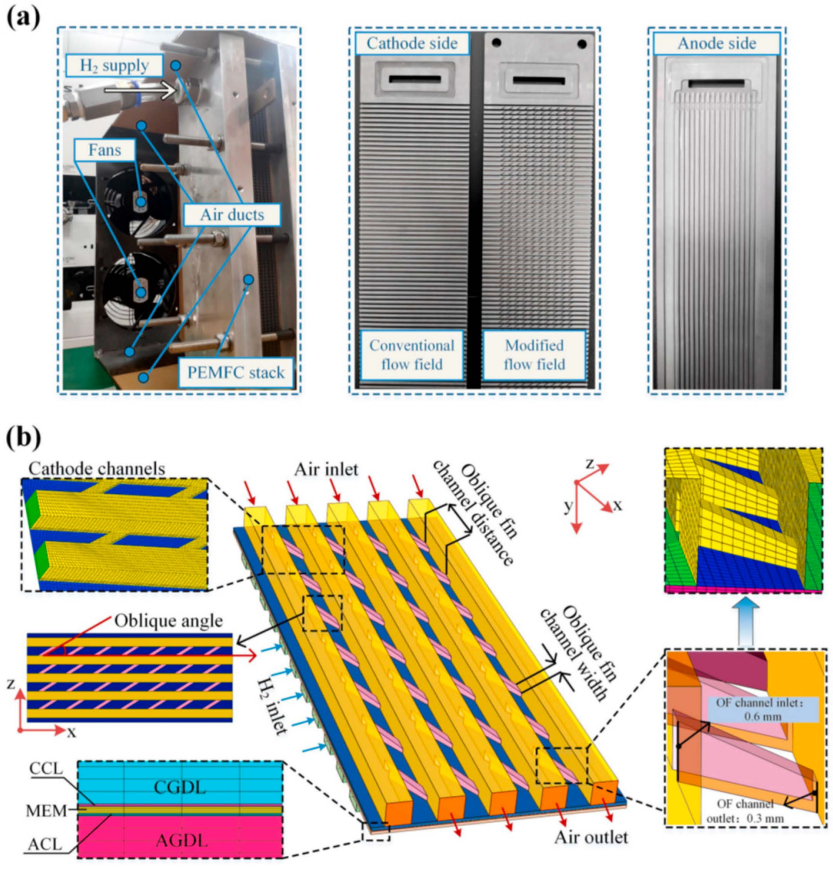

Figure 3. (**a**) Photos of the air-cooled PEMFC of the experimental test system and BPs and (**b**) schematic diagram of the computational domain and meshing details in numerical simulations [119]. Reproduced with permission from Elsevier.

2.3. Inovative Flow Fields

Chen et al. [121] introduced an innovative tree-shaped fractal cooling flow field for bipolar plates in fuel cells, drawing inspiration from the microstructure of biomimetic leaves and featuring varying dimensions (Figure 4). Their findings indicate that this bio-inspired cooling flow field provides superior coolant distribution and improved temperature uniformity compared to traditional parallel cooling flow fields. Furthermore, when compared to serpentine cooling flow fields, the tree-shaped fractal design effectively addresses the issue of excessive cooling pressure drops and minimizes parasitic power losses while maintaining efficient cooling performance. This novel design presents a promising solution for mitigating localized overheating in PEMFCs.

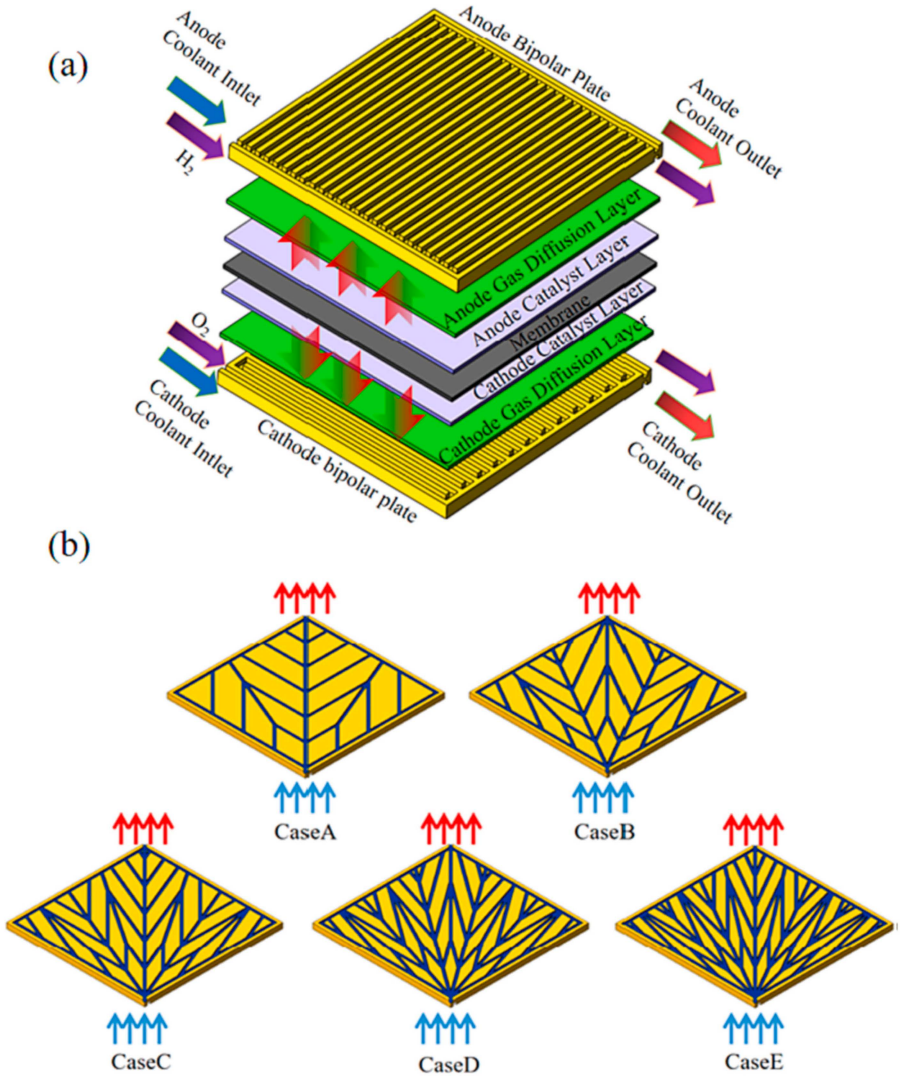

Figure 4. Fuel cell geometry: (**a**) schematic diagram of the PEMFC and (**b**) tree-shaped fractal cooling flow field [121]. Reproduced with permission from Elsevier.

Liu et al. [122] investigated three biomimetic cooling channel designs based on the heat dissipation characteristics of human capillaries. To precisely evaluate fluid distribution and heat transfer within these channels, they employed a three-dimensional flow model, comparing the cooling performance of the biomimetic capillary cooling channels with that of conventional parallel channels. Their results show that the topology-optimized biomimetic cooling channels can significantly improve overall cooling performance.

Zhang et al. [123] conducted a numerical investigation on a serpentine cooling channel featuring dimples to enhance the internal thermal management of proton exchange membrane fuel cells (Figure 5). They compared three types of cooling channels: an elliptical dimple cooling channel, a circular dimpled cooling channel, and a smooth cooling channel. Their findings demonstrate that the elliptical dimple cooling channel outperforms the other two configurations due to the narrower surface area of the elliptical dimple, which improves fluid flow and creates a vortex trailing edge that facilitates heat exchange. Additionally, when the optimal dimple dimensions are utilized, the elliptical dimple cooling channel effectively reduces the maximum temperature while also decreasing pressure drops.

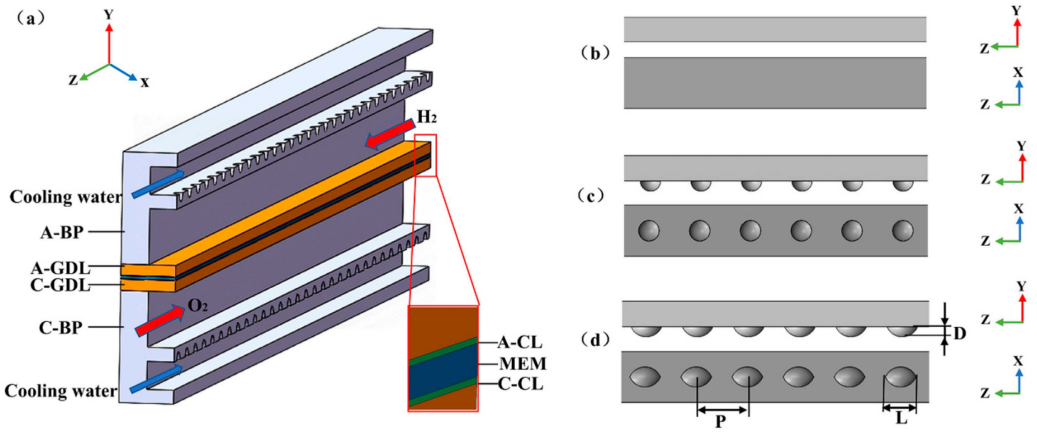

Figure 5. (**a**) PEMFC model; (**b**) smooth cooling channel; (**c**) circular dimpled cooling channel and (**d**) elliptical dimple cooling channel [123]. Reproduced with permission from Elsevier.

However, the authors did not address the manufacturing challenges associated with implementing these designs on a larger scale compared to conventional designs.

2.4. Constrained Flow Fields

As indicated by Poirot-Crouvezier and Roy [124], the use of metallic bipolar plates obtained from stamped thin foils can produce complicated coolant flow fields, which are rarely studied in the literature. Indeed, in such bipolar plates, the cooling circuit results from the overlapping of the ribs of the anode flow field and the ribs of the cathode flow field. If the anode and cathode flow fields are not wavy or parallel, but rather serpentine or interdigitated, the cooling flow field contains linear channels in different orientations, chaotic connections, and eventually flow blockages. Consequently, uniform coolant distribution is not reachable with such bipolar plates. Therefore, a common and simultaneous optimization of the three fluid circuits has to be conducted in order to reduce the temperature heterogeneity as much as possible. Furthermore, experimental and numerical analyses of the thermal behaviour of such cells are necessary to correctly apprehend their performance and lifetime [125].

To overcome this issue, Mahdavi et al. [126] proposed the incorporation of an intermediate "spacer plate" which facilitates the cooling fluid's passage through the cooling flow field, promoting uniform temperature distribution. They numerically designed three spacer plates, labelled A, B, and C. Their results indicated that model C performed best, exhibiting the lowest surface-averaged temperature among the designs. To further improve cooling, additional modifications to model C were explored by adding some holes in critical areas of the spacer plate to reduce the maximum temperature. It was shown that the modified spacer plate C was successfully optimized, achieving a better cooling efficiency.

Rahimi-Esbo et al. [127] conducted a numerical study on a serpentine design for the reactant flow field of a PEMFC, incorporating a spacer plate between the bipolar plates

(Figure 6a). They evaluated several configurations, progressing from an initial design without a spacer to an optimized geometry (design 8) by adjusting the placement and number of spacers (Figure 6b). The results indicated that, in the absence of a spacer, cooling fluid tended to become trapped in some regions of the bipolar plate. Therefore, they used, at first, a simple spacer with parallel rectangular holes (design 1). They observed high contact resistance for this design with an IUT of 2.09 °C and an average temperature of 73.88 °C. They then iteratively refined the design by analyzing the IUT (Figure 6c) and temperature contour on the spacer surface at each step to reach the lowest IUT (1.45 °C) with their optimized design.

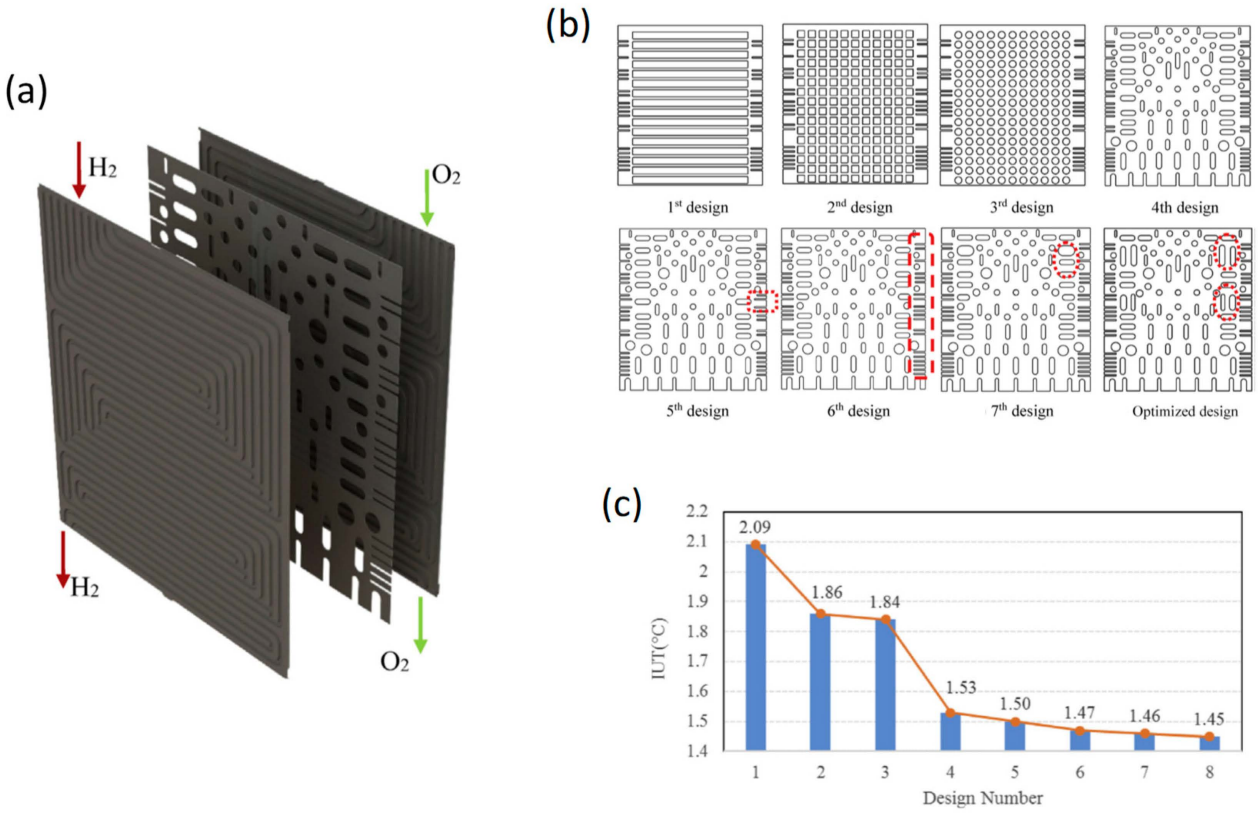

Figure 6. (**a**) Location of the spacer between two bipolar plates; (**b**) the design steps of a spacer from the first design to the optimized design; and (**c**) IUT obtained according to the different spacer designs [127]. Reproduced with permission from Elsevier.

3. Coolant Operation

Many studies investigate the influence of the cooling flow-field design, but other authors have also considered the effects of the coolant's operation, including the coolant flow velocity and temperature gradient.

3.1. Effect of Coolant Flow Velocity

Song et al. [114] studied the maximum temperature, temperature difference, temperature uniformity index and pressure drop of the multi-channel cooling plate under varying liquid-coolant inlet flow rates by numerical simulation (Figure 7). Overall, they found that the temperature of the cooling plate decreases as the total inlet coolant flow increases, especially in designs with less efficient cooling processes. However, when the flow channel is excessively long, it can substantially increase the pressure drop, potentially leading to fluid blockage.

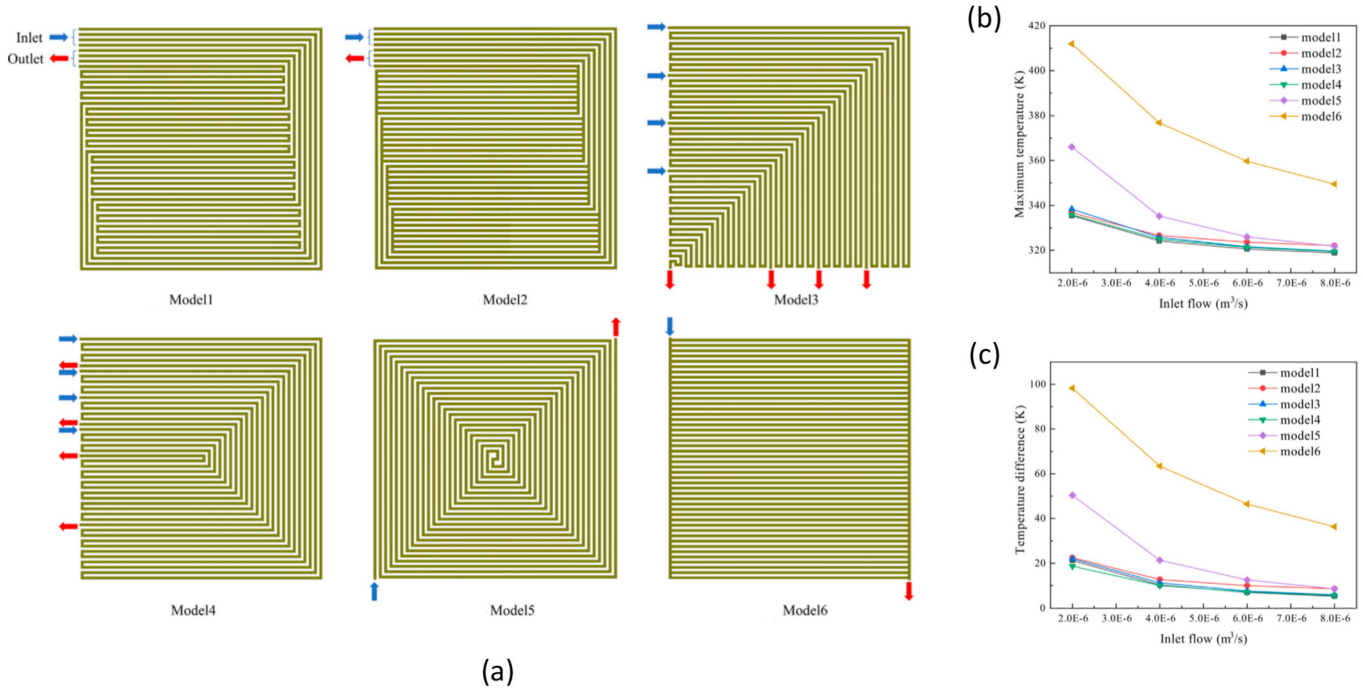

Figure 7. (**a**) Design scheme of flow field. Effect of inlet flow on heat transfer characteristics; (**b**) maximum temperature and (**c**) temperature difference [114]. Reproduced with permission from Elsevier.

Liu et al. [115] validated previous findings with a multi-phase numerical study of a large-scale PEMFC analyzing three CFF designs (Figure 8a). Although increasing the cooling flow rate reduced the IUT and increased the current density of the cell, they noticed a risk of flooding near the cathode outlet for excessive flow rate (Figure 8b). Moreover, the benefits in temperature uniformity and current density became less pronounced at higher flow rates. Consequently, they recommended a moderate flow rate, as high flow rates significantly increase the pressure drop, leading to a substantial increase in the pumping power needed (Figure 8c).

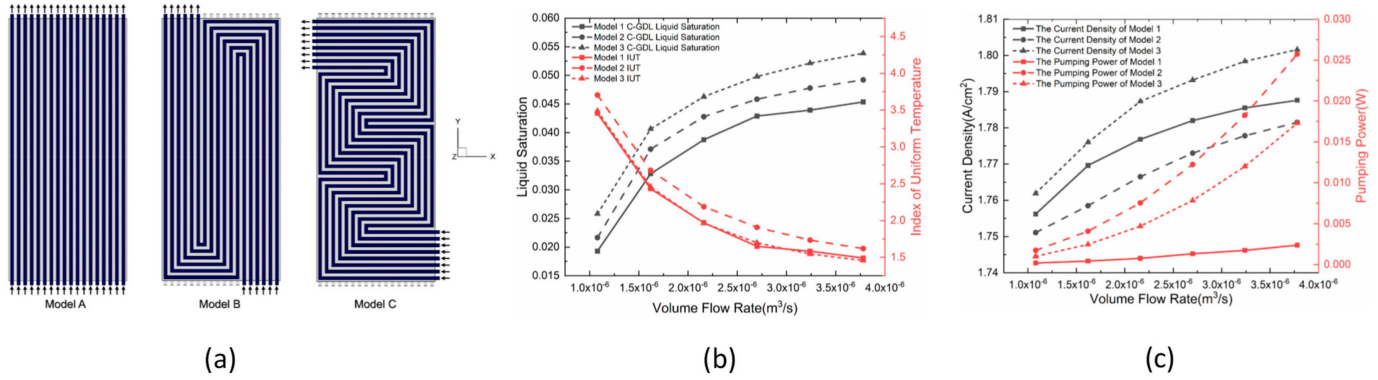

Figure 8. (**a**) Three coolant flow-field designs for large-scale PEMFCs; (**b**) average cathode liquid saturation and index of uniform temperature profile for the PEMFC under different cooling water inlet volume flow rates; and (**c**) average current density profile and pumping power profile under different coolant volume flow rates [115]. Reproduced with permission from Elsevier.

Recent studies have also examined the effect of coolant flow velocity in a serpentine CFF with an optimized spacer plate [127], wavy CFF [117], and fractal CFF [121], all using numerical simulations. These studies consistently found that increasing the inlet coolant flow velocity enhances the cooling process but can lead to a significant pressure

drop. Additionally, they noted that once the flow velocity reaches a certain threshold, a further increase has minimal impact on the cell. Consequently, they suggested that the highest coolant flow rate may not be the optimal choice, as it requires balancing temperature distribution with pump output power. A systems-level approach is therefore recommended.

Xu et al. [128] investigated the effect of steady or pulsating coolant flow with bionic tree-like microchannels by simulation with a 2D thermal model. They concluded that pulsating flow could improve the IUT compared to a steady coolant flow rate, due to a reduced boundary layer.

Nandjou et al. [125] developed a physics-based model to study variations in temperature, humidity, and current density across a large-area PEM fuel cell. To measure temperature and current density under real operating conditions, they used a printed circuit board with an S++ sensor plate placed between two monopolar plates at the centre of a 30-cell stack with an active area of 220 cm^2. The model accurately predicted temperature and current density distributions when comparing computed and experimental data. In a follow-up study, Nandjou et al. [129] explored how the cooling flow velocity impacts temperature and current density distributions under varying operating conditions (Figure 9). Their model revealed that the multi-serpentine channels used for reactant flow create a complex, chaotic cross-flow cooling field, which induces significant spatial heterogeneities in local conditions, accelerating cell component degradation. The findings showed that cooling flow is the primary factor affecting temperature distribution. Specifically, the membrane exhibited a hotspot reaching approximately 94 °C, compared to the operating temperature of 80 °C regulated at the stack outlet, due to the decrease in the cooling flow velocity in this region, from about 0.3 $m{\cdot}s^{-1}$ to 0.03 $m{\cdot}s^{-1}$ (Figure 9). In contrast, variations in local current density had a comparatively smaller impact on temperature distribution.

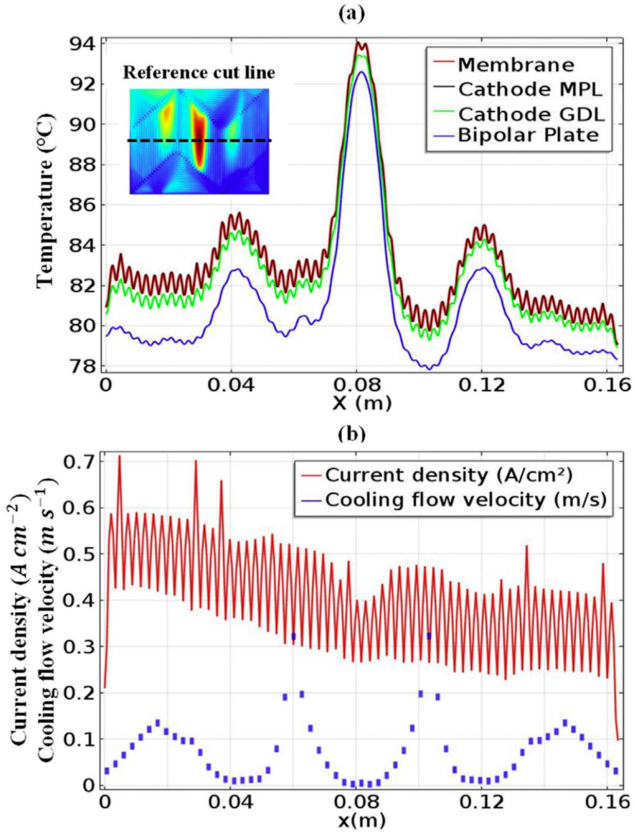

Figure 9. (**a**) Temperature distribution at the reference cut line in the membrane, cathode microporous layer, cathode gas diffusion layer and bipolar plate for a current density of 0.42 A cm^{-2} and (**b**) current density and cooling flow velocity at the cut line [129]. Reproduced with permission from Elsevier.

Building on previous work, Tardy et al. [69] applied the prior model to investigate water management considering the real bipolar plate design. To validate their results, they compared the liquid water thickness distribution predicted by their model with neutron imaging measurements obtained at the National Institute of Standards and Technology (NIST) for a stack of five cells. At low current densities, the model successfully and quantitatively reproduced the regions of liquid water accumulation within the stack (Figure 10). Finally, they observed a greater accumulation of liquid water in the cooler regions, consistent with the temperature distribution predicted by Nandjou et al. [125,129].

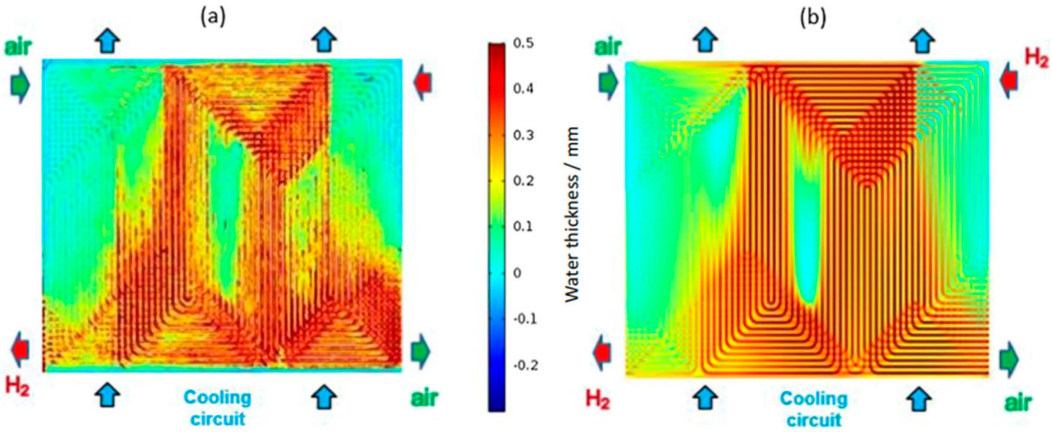

Figure 10. (**a**) Measured and (**b**) simulated total liquid water thickness for a stack of 5 cells for a current density of 0.25 A cm^{-2} and for an inlet cooling water temperature of 64 °C [69]. Reproduced with permission from Elsevier.

3.2. Effect of Coolant Temperature Gradient

As shown in the previous sections of this review, studies focus mainly on the structural parameters associated with the coolant (flow-field design and flow configuration) and primarily seek a uniform temperature distribution. They do show that a high flow rate may not be of interest in terms of system efficiency and that coolant flow configuration influences the temperature and water distribution. However, they do not try to find a more optimal coolant flow rate and do not study the effect of the cooling water parameters (flow rate, inlet temperature and flow configuration) as a whole. Indeed, the operation of the coolant, meaning its operating temperature and flow rate, influences the heat exchange between the BP and the coolant and, as a result, the temperature distribution and operating temperature of the cell. This last section investigates the coolant flow direction compared to the air or hydrogen one and the coolant temperature gradient in parallel flow configuration.

Shen et al. [130] introduced three innovative cooling modes (Figure 11) designed to enhance heat distribution within a PEM fuel cell, offering alternatives to the traditional unidirectional cooling flow (Model A): reverse flow cooling in the interlayer channel (Model B), reverse flow cooling in adjacent channels (Model C), and bidirectional circulation cooling (Model D). In Model D, the cooling water flow direction periodically alternates, which indicates that all are inlet at T and all switch to outlet at 2T. Based on their results, compared to Model A, Model B shows only minor improvements in temperature distribution and performance. However, both Model C and Model D significantly enhance temperature distribution, resulting in higher power density and efficiency. Indeed, the maximum temperature difference is reduced by 4.3 K and 3.2 K for Models C and D, respectively, compared to Model A. Moreover, the power density of Models C and D increases by 23% and 20.6%, respectively, compared to the traditional cooling flow, when operating at a

voltage of 0.65 V. Additionally, the commutation time affects temperature distribution, especially at higher commutation frequencies.

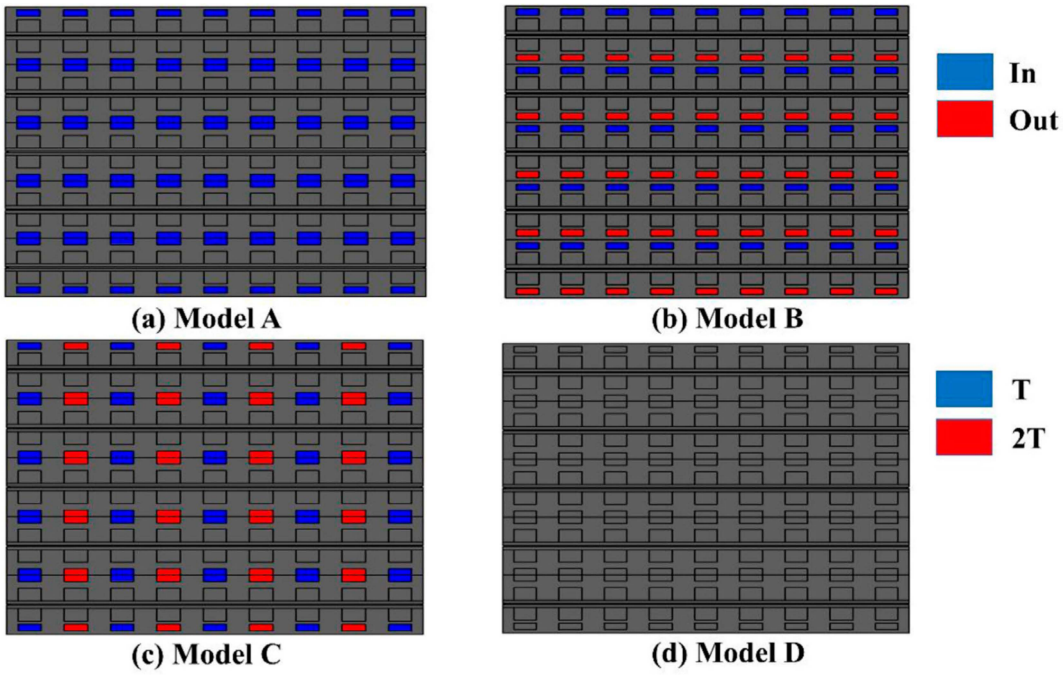

Figure 11. Cooling schemes of each model: (**a**) traditional unidirectional cooling flow (Model A); (**b**) reverse flow cooling of the interlayer flow channel (Model B); (**c**) reverse flow cooling of the adjacent channel (Model C;) and (**d**) bidirectional circulation cooling (Model D) [130]. Reproduced with permission from Elsevier.

Chen et al. [117] studied wavy flow fields using 3D simulation of one cell. They noted that when the coolant is introduced in the same direction as oxygen, the temperature distribution is more uniform, and the performance is increased at high current density. On the contrary, when the coolant and hydrogen are introduced in the same direction, a higher temperature gradient is observed. In their numerical study, Zhang et al. [131] studied the effect of the direction of the coolant using a large-scale multi-phase model. Based on their simulations of the liquid water distribution at the different layers of the cell, they conclude that, for a counter-current gas flow configuration, the coolant must flow in the same direction as the air flow. Indeed, this configuration avoids the accumulation of liquid water at the cathode outlet in the cathode catalyst layer and at the interface between the cathode catalyst layer and gas diffusion layer. Finally, Morin et al. [55] also emphasize the impact of the flow configuration on the distribution of liquid water content, which is linked to the current density distribution. Their study employed a P3D model and data from neutron imaging to analyze the current density, temperature and liquid water content distributions and concluded that best performances are obtained for the counter-flow configuration, especially with the coolant in the same direction as the air.

Very few research works have studied the effect of the coolant flow rate coupled with its inlet or outlet temperature. Amirfazli et al. [132] numerically studied the effect of the coolant flow rate on the uniformity temperature distribution for different manifold cross sectional areas. They showed that the uniformity of the temperature distribution increases systematically with the coolant flow rate. They concluded that it is beneficial to increase the flow rate but that it can lead to higher parasitic losses caused by excessive coolant pumping. However, this study assumes that the most uniform temperature distribution possible is desirable. Moreover, it is carried out at a constant coolant inlet temperature of 46 °C for a cell voltage of 0.6 V and a stack output current of 220 A.

Liu et al. [115] studied the effect of the coolant by (1) keeping the coolant flow rate constant for three different coolant flow-field designs and (2) varying the flow rate while keeping the coolant inlet temperature at 70 °C with a large-scale cell, non-isothermal and 3D model. They found that the PEMFC operating temperature is determined by the chosen coolant inlet temperature and that a higher PEMFC operating temperature reduces the risk of flooding. They also found that the coolant flow rate impacts the temperature gradient of the PEMFC between the inlet and the outlet for a constant inlet coolant temperature, and that maximal temperature distribution uniformity can lead to liquid water accumulation in the gas diffusion layers. They conclude that an optimal coolant flow rate can simultaneously decrease the risk of flooding and the pump power consumption.

Finally, Cornet et al. [133] numerically tested over a hundred operating conditions on a 250 cm^2 PEMFC operating in counter-flow with the coolant in the same direction as the air. These operating conditions include variation in coolant temperature outlet and coolant temperature gradient between the cell inlet and outlet (meaning a variation in the coolant flow rate to maintain the outlet temperature and the coolant temperature gradient). In a general way, the increase in coolant outlet temperature and coolant temperature gradient limits both drying and flooding of certain areas of the cell. Among all the simulated results, the two highlighted polarization curves indicate that increasing the coolant temperature gradient (i.e., decreasing the coolant flow rate) while lowering the coolant outlet temperature can enhance the cell's performance at current densities above 1.5 A/cm^2 (Figure 12a). Indeed, a higher coolant temperature gradient allows for lower cell temperature at the air inlet, improving the membrane hydration in this area which is usually subject to drying (Figure 12b). A higher coolant outlet temperature enables an increase in the cell's operating temperature, which improves performance in the activation zone at low current densities but reduces performance at high current densities (Figure 12a) due to membrane drying (Figure 12b). A higher temperature gradient also implies a smaller coolant flow rate, limiting the power consumption of the coolant pump. Optimizing these two parameters together is therefore beneficial for both cell performance and system efficiency.

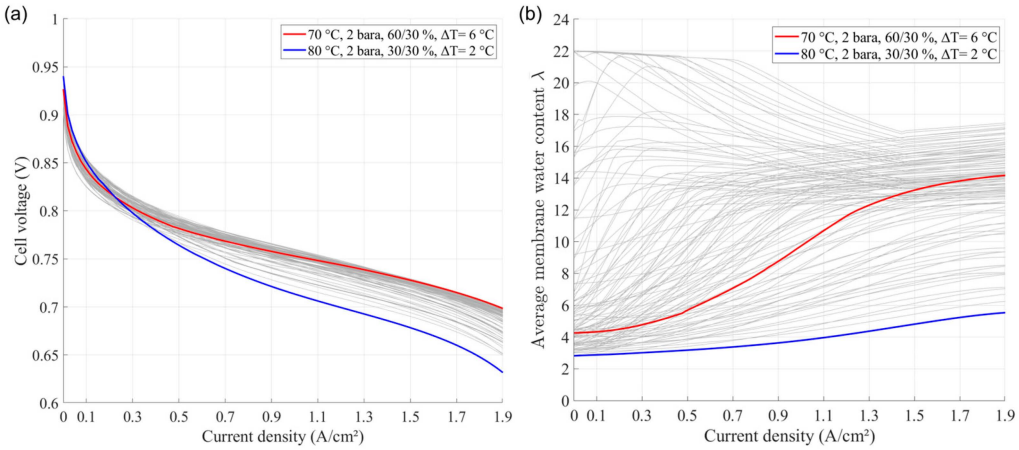

Figure 12. (**a**) I–V curves and (**b**) averaged water content obtained for the 108 simulations with the calibrated spatially averaged P3D model featuring a variation in coolant outlet temperature (60 °C, 70 °C and 80 °C), in coolant temperature gradient between inlet and outlet ΔT (2 °C, 6 °C, 10 °C and 20 °C) and in anode and cathode RH (30%, 50% and 60%). The best (red) and the worst (blue) performances at high current density have been highlighted.

The coolant operation has a direct impact on the temperature distribution in the cell, which itself impacts the humidity distribution and, therefore, the cell performance. It also impacts the consumption of the cooling pump and therefore the efficiency of the whole

system. Yet, little research has been carried out on the coupled effect of coolant temperature and the temperature gradient between the inlet and outlet.

4. Ageing

Many phenomena can contribute to the ageing of a PEMFC [40,134,135]: corrosion of the carbon support of the electrodes, chemical degradation of the membrane or the ionomer of the active layers, dissolution of the platinum, etc. It is worth mentioning that ageing studies are generally carried out using small single cells (25 cm^2 or less), placed under a variety of conditions. Experiments on segmented cells have shown the relevance of this technique for understanding such mechanisms [136]. Few studies have been carried out on the scale of a complete stack, where all the phenomena are coupled (thermal, fluidic, etc.) [67,137–141]. Since lifespan remains a major challenge for the commercialization of PEMFCs, understanding their ageing process is crucial for prognosis and health management. This enables proactive interventions to prevent fuel cell failures and, ultimately, extends the operational life of PEMFCs. Most of the parameters influencing degradation kinetics must be considered on a local scale, since operating heterogeneities can have a major impact on ageing. Given the diversity of the mechanisms involved, ageing is influenced by the size of the PEMFCs under consideration and by the way they are stressed. As a result, any durability study begins by selecting the operating parameters to be maintained over several hundred hours, under either steady or variable conditions, including start-up and shutdown phases. Given the long duration of these tests, the specific study of certain degradation mechanisms can be approached with shorter tests [67,141–143], named accelerated stress tests. At the end of these tests, studies are often completed with post mortem analyses realized at different locations in the active area [144]: optical, SEM or TEM visualizations with layer thickness measurements, contact angle measurements, element distribution measurements, etc.

The stresses applied to the stacks undergoing ageing tests are generally defined according to the intended application. The first tests are carried out at constant current, often at the nominal operating point. The degradations that appear during this type of test, particularly those that are reversible, are not necessarily representative of those encountered when the operating parameters vary over time, as in the real application. The latter causes a drop in cell voltage that can be recovered, for example during a simple start up or shut down or characterization protocol. The recovery of reversible voltage loss through polarization curve tests and other interventions results in intermittent performance degradation. To address this challenge, Meng et al. [145] proposed a novel health indicator that significantly minimizes its dependence on current density, providing a more accurate reflection of fuel cell status. It differs from so-called 'irreversible' degradation, which corresponds to a reduction in performance that no regeneration protocol can reverse [146]. As a result, variable stress profiles have been defined to investigate the impact of an air supply fault [147] or the impact of alternating fuel feeding [140]. Moreover, many have focused on performance degradation during start-up/shut-down phases [148,149]. Other mechanisms, such as membrane degradation, have been the subject of analyses linking operating conditions to the location of degradation [150].

Studies in large cells of the degradation phenomena can be conducted at a local scale with current scan sensors, such as S++ boards, which are able to measure surface mappings of current density and temperature over the active area. It can be employed in large single cells, like in the work of Lochner et al. [138], where real stamped metallic bipolar plates, similar to the ones used in stacks, are used in a single cell equipped with a current scan sensor and subjected to durability tests (Figure 13). Their results show that, depending on the location of the active area, different degradation behaviour occurs, leading to an

evolution of the current density distribution. At the end of the test, in this case where water flooding occurs frequently, a part of the cell produces a current density close to zero. This validates the use of real components in single cells, providing a single cell hardware closer to a stack hardware than classical segmented single cells that use machined flow-field plates. However, in this study, the in-plane temperature gradient through the cell remains lower than 1.5 °C, due to a fixed high coolant flow rate. One can estimate that it has an impact on water flooding, which is, in this study, a major cause of cell degradation.

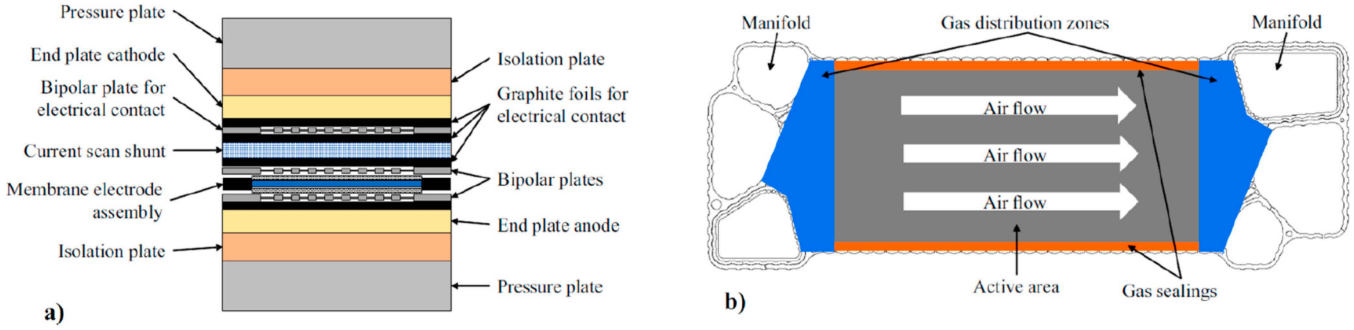

Figure 13. Example of single cell hardware using real bipolar plates and current scan sensor: (**a**) sectional view of the cell and (**b**) air side of the bipolar plate. The airflow direction in the straight channels is indicated by white arrows [138]. Reproduced with permission from Elsevier.

Lochner et al. [151] propose a review focused on the effect of temperature on the degradation phenomena in PEMFC. To gain insight into the location of the degradations, the authors observe that ex situ studies are numerous, such as post-mortem analyses of degraded components. However, regarding in situ studies, they note that the in-plane distribution of temperature in stacks is generally unknown, impeding the validation of local improvements in cells' materials.

As discussed in the previous sections, the current density distribution depends on the local gas composition and water content and, to a lesser extent, the local temperature. A variation in this distribution during cell ageing can have an impact on degradation. Knowledge of this variation can lead to ways of increasing durability, as shown recently by Chandesris et al. [152]. As shown in the literature [137–139], the current density distribution can vary differently depending on the operating conditions. Nevertheless, local temperature could be a driving force for many degradation mechanisms. For example, the loss of hydrophobicity of gas diffusion layers is promoted by high temperature and by the presence of large and variable amounts of liquid water [153].

To delve further into the understanding of the coolant flow effect, Nandjou et al. [67] proposed an accelerated stress test based on the standard Fuel Cell Dynamic Load Profile derived from New European Driving Cycle in the frame of the FCH-JU 303445 StackTest project [154]. This incorporated a variation in relative humidity in addition to a variation in current in order to consider the reduced efficiency of high-power humidifiers. The stack used for the durability test presented serpentine flow fields at the anode and cathode. Post-mortem analyses of the aged membrane–electrode assemblies and bipolar plates were conducted at the end-of-life. The experimental findings were then compared with the simulated temperature, humidity, and membrane water content within the cell. In this study, a detailed analysis of the influence of local temperature and humidity on PEMFCs' degradations was performed. The tests carried out, in the absence of start-up and shut-down phases, correspond to stresses on the cell that do not favour carbon corrosion or loss of active surface area. Detailed observation of the corrosion on the stamped metallic bipolar plates was performed. The location of the corrosion marks was recorded for all the

bipolar plates and a statistical analysis was carried out. This provided the most frequent location of corrosion marks on the active surface. For the anode, these coincided with the areas of highest temperature on the active surface. For the cathode, they coincided with the areas where the humidity in the cathode channels was highest, according to the results of the pseudo-3D model. The measurement of fluorine in the effluent, as the test progresses, provided an indicator of chemical attack on the membrane [155]. There was a major difference between the steady-state and dynamic tests. Indeed, the fluoride release was around ten times greater in the dynamic test, indicating greater degradation of the membrane material (Figure 14). As a result of ageing, structural degradation of the membrane occurred in certain well-defined areas of the active surface. The SEM observation showed that this was delamination of the material. The defects were located mainly in front of the rib, as shown by microscopic observation. Both the anode and cathode designs were visible, with the cathode predominating.

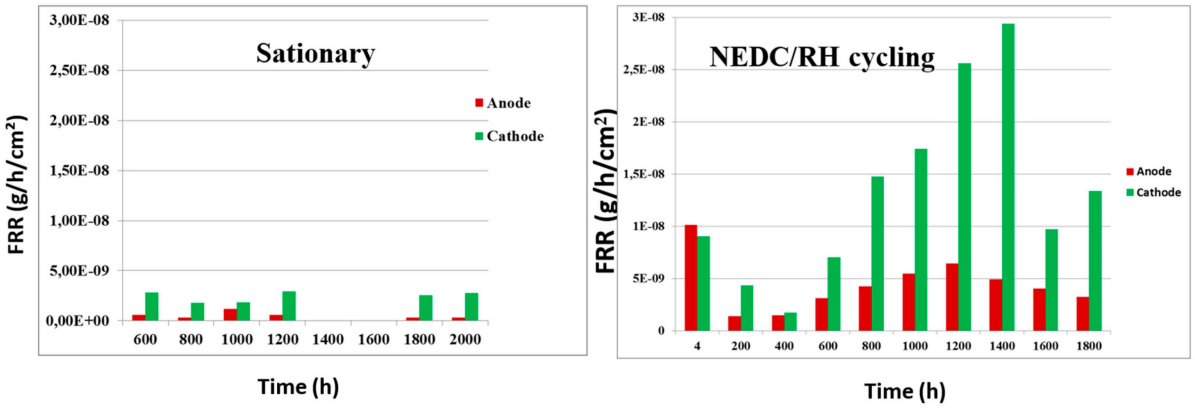

Figure 14. Evolution of the fluorine release rate [156].

Among the numerous local degradations observed in Figure 15, only elevated local temperature can be identified as the main factor promoting anode plate degradation. Nevertheless, the membrane degradation is indirectly linked to the local temperature. Indeed, the occurrence of membrane pinholes and micro-cracks, responsible for a sudden loss of functionality of the cells, is correlated with the amplitude of the local water content variation induced by the current density and temperature variation. Therefore, the local degradation phenomena are deeply related to the reactive gasses and cooling flow-field designs.

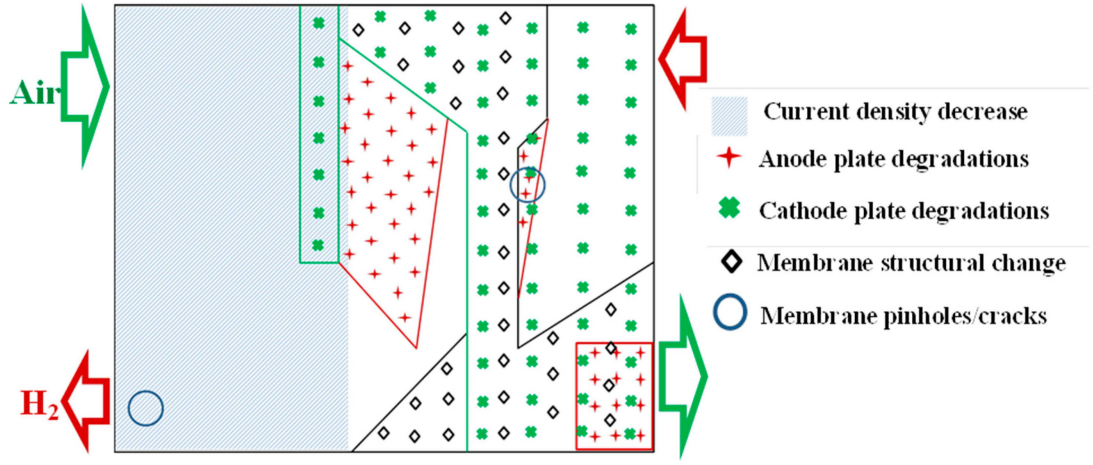

Figure 15. Overview of the observed degradations. [67]. Reproduced with permission from Elsevier.

5. Conclusions

The primary technical challenges in developing PEMFCs are closely related to the management of temperature and water within the stack, as performance and degradation are inherently dependent on local temperature and humidity conditions. Nowadays, the reference temperature is 80 °C and the reference relative humidity values vary between 30 and 50%. However, there is an important push to higher temperature, in order to decrease the weight, volume and cost of the cooling devices. Moreover, further simplification of the fuel cell system is desirable, involving a suppression of the air external humidification. In this context, the precise control of the maximum cell temperature is of paramount importance to prevent membrane drying (which reduces ionic conductivity) and to minimize component ageing. Therefore, thorough investigations are essential to tackle the specific challenges of heat and water management within the cell and to understand their impact on degradation.

Experimental methods are valuable for studying temperature and water distribution within the cell, but they are often limited by the high cost and invasiveness of measurement techniques. In the literature, printed circuit boards emerge as the most practical choice for local measurements due to their high resolution and accuracy, coupled with relatively low invasiveness compared to other available technologies. Another solution consists of the development of a physics-based model, with the resolution at the same time of the heat sources and cooling water heterogeneities. The challenge for these models lies in achieving an optimal balance between the dimensionality of its description, the accuracy in representing physical phenomena, and the computational efficiency. Ideally, the model should operate at the cell scale to capture all global heterogeneities within the fuel cell components. Additionally, it should enable predictions of temperature, humidity, and related parameters across each component of the cell.

A review of the literature on operating heterogeneities shows that sensitivity studies on current density distribution are often based on a limited number of operating conditions and that the numerical studies mostly neglect the influence of coolant operation with the associated temperature gradient. Most of the works focus on the impact of the coolant flow-field design and the operating conditions on the current density distribution.

The BP design largely influences the coolant flow distribution, leading to hot spots deeply affecting the water content and relative humidity distributions. The cooling flow field has proven to be a crucial factor in heat management, highlighting the importance of careful attention to its design.

The operating conditions imposed on the stack also have a clear influence. Hence, increasing the operating current induces more temperature heterogeneities, emphasizing the hot spots. Conversely, the increase in the coolant flow rate enables one to reduce the temperature difference between the inlet and the outlet of the cooling water. Furthermore, in automotive conditions, the cycling of operating parameters imposed on the stack induces a non-uniform cycling of the local operating conditions inside the stack, which can lead to membrane degradation.

This review highlights the significance of the coolant temperature gradient between the coolant inlet and outlet. Indeed, an increase in the coolant temperature gradient (which corresponds to a reduction in the coolant flow rate) combined with an increase in operating temperature enhances the cell's performance at a given current density. The control of this parameter is closely linked to the balance of the plant of the system, because it depends on the flow provided by the coolant pump and on the performance of the heat exchanger. On the other hand, innovative architectures of the cooling circuit inside the stack targeting a reduction in this gradient are likely to increase the mass and volume of the stack. Consequently, a decrease in the coolant temperature gradient can be associated with a decrease in the power density of the system, which is often not desirable in automotive

applications but could be acceptable for some heavy-duty transport, railway, maritime or industrial applications.

Some ageing studies have been carried out to investigate the influence of the cooling flow-field design and configuration but none are dedicated to the influence of the coolant temperature gradient. This work suggests that additional durability studies should be conducted in future research, focusing on the application of a high coolant temperature gradient (by decreasing the coolant flow velocity) across various operating points, in particular since it remains unclear whether alterations in the profiles of current density production over the active surface area, resulting from the compensatory effects of current production areas, may influence the durability of the cell.

Author Contributions: Conceptualization, M.C., E.T. and J.-P.P.-C.; methodology, J.-P.P.-C. and Y.B.; formal analysis, M.C., E.T. and J.-P.P.-C.; investigation, M.C., E.T. and J.-P.P.-C.; data curation, M.C., E.T. and J.-P.P.-C.; writing—original draft preparation, E.T. and Y.B.; writing—review and editing, M.C., E.T., J.-P.P.-C. and Y.B.; visualization, E.T.; supervision, J.-P.P.-C. and Y.B. All authors have read and agreed to the published version of the manuscript.

Funding: This research received no external funding.

Conflicts of Interest: The authors declare no conflicts of interest.

Nomenclature

BP	Bipolar plate
CFF	Cooling flow field
IUT	Index of uniform temperature
PEM	Proton exchange membrane
PEMFC	Proton exchange membrane fuel cell
RH	Relative humidity

References

1. Veziroğlu, T.N.; Şahın, S. 21st Century's Energy: Hydrogen Energy System. *Altern. Energy Ecol. ISJAEE* **2019**, *4–6*, 14–27. [CrossRef]
2. Luo, X.; Wang, J.; Dooner, M.; Clarke, J. Overview of Current Development in Electrical Energy Storage Technologies and the Application Potential in Power System Operation. *Appl. Energy* **2015**, *137*, 511–536. [CrossRef]
3. U.S. Department of Energy. Comparison of Fuel Cell Technologies. Available online: https://www.energy.gov/eere/fuelcells/articles/comparison-fuel-cell-technologies-fact-sheet (accessed on 4 November 2024).
4. European Hydrogen Observatory, Hydrogen Value Chains. Available online: https://observatory.clean-hydrogen.europa.eu/learn-about-hydrogen/hydrogen-basics/hydrogen-value-chains (accessed on 4 November 2024).
5. Migliardini, F.; Capasso, C.; Corbo, P. Optimization of Hydrogen Feeding Procedure in PEM Fuel Cell Systems for Transportation. *Int. J. Hydrogen Energy* **2014**, *39*, 21746–21752. [CrossRef]
6. Migliardini, F.; Di Palma, T.M.; Gaele, M.F.; Corbo, P. Hydrogen Purge and Reactant Feeding Strategies in Self-Humidified PEM Fuel Cell Systems. *Int. J. Hydrogen Energy* **2017**, *42*, 1758–1765. [CrossRef]
7. Marx, N.; Hissel, D.; Gustin, F.; Boulon, L.; Agbossou, K. On the Sizing and Energy Management of an Hybrid Multistack Fuel Cell—Battery System for Automotive Applications. *Int. J. Hydrogen Energy* **2017**, *42*, 1518–1526. [CrossRef]
8. Marx, N.; Hissel, D.; Gustin, F.; Boulon, L.; Agbossou, K. On Maximizing the Steady-State Efficiency of a Multi-Stack Fuel Cell System. In Proceedings of the 2018 IEEE Vehicle Power and Propulsion Conference (VPPC), Chicago, IL, USA, 27–30 August 2018; IEEE: Chicago, IL, USA, 2018; pp. 1–6.
9. Rodosik, S.; Poirot-Crouvezier, J.-P.; Bultel, Y. Impact of Humidification by Cathode Exhaust Gases Recirculation on a PEMFC System for Automotive Applications. *Int. J. Hydrogen Energy* **2019**, *44*, 12802–12817. [CrossRef]
10. Rodosik, S.; Poirot-Crouvezier, J.-P.; Bultel, Y. Simplified Anode Architecture for PEMFC Systems Based on Alternative Fuel Feeding: Experimental Characterization and Optimization for Automotive Applications. *Int. J. Hydrogen Energy* **2020**, *45*, 19720–19732. [CrossRef]
11. Shang, Z.; Hossain, M.M.; Wycisk, R.; Pintauro, P.N. Poly(Phenylene Sulfonic Acid)-Expanded Polytetrafluoroethylene Composite Membrane for Low Relative Humidity Operation in Hydrogen Fuel Cells. *J. Power Sources* **2022**, *535*, 231375. [CrossRef]

12. Bhatia, D.; Sabharwal, M.; Duelk, C. Analytical Model of a Membrane Humidifier for Polymer Electrolyte Membrane Fuel Cell Systems. *Int. J. Heat Mass Transf.* **2013**, *58*, 702–717. [CrossRef]
13. Coralli, A.; Sarruf, B.J.M.; De Miranda, P.E.V.; Osmieri, L.; Specchia, S.; Minh, N.Q. Fuel Cells. In *Science and Engineering of Hydrogen-Based Energy Technologies*; Elsevier: Amsterdam, The Netherlands, 2019; pp. 39–122, ISBN 978-0-12-814251-6.
14. Chang, Y.; Qin, Y.; Yin, Y.; Zhang, J.; Li, X. Humidification Strategy for Polymer Electrolyte Membrane Fuel Cells—A Review. *Appl. Energy* **2018**, *230*, 643–662. [CrossRef]
15. Kim, B.J.; Kim, M.S. Studies on the Cathode Humidification by Exhaust Gas Recirculation for PEM Fuel Cell. *Int. J. Hydrogen Energy* **2012**, *37*, 4290–4299. [CrossRef]
16. Hu, J.; Xu, L.; Li, J.; Ouyang, M.; Cheng, S.; Fang, C. Water Management in a Self-Humidifying PEM Fuel Cell System by Exhaust Gas Recirculation. In Proceedings of the 2014 IEEE Conference and Expo Transportation Electrification Asia-Pacific (ITEC Asia-Pacific), Beijing, China, 31 August–3 September 2014; IEEE: Beijing, China, 2014; pp. 1–6.
17. Jiang, H.; Xu, L.; Fang, C.; Zhao, X.; Hu, Z.; Li, J.; Ouyang, M. Experimental Study on Dual Recirculation of Polymer Electrolyte Membrane Fuel Cell. *Int. J. Hydrogen Energy* **2017**, *42*, 18551–18559. [CrossRef]
18. Xu, L.; Fang, C.; Hu, J.; Cheng, S.; Li, J.; Ouyang, M.; Lehnert, W. Self-Humidification of a Polymer Electrolyte Membrane Fuel Cell System With Cathodic Exhaust Gas Recirculation. *J. Electrochem. Energy Convers. Storage* **2018**, *15*, 21003. [CrossRef]
19. Migliardini, F.; Unich, A.; Corbo, P. Experimental Comparison between External and Internal Humidification in Proton Exchange Membrane Fuel Cells for Road Vehicles. *Int. J. Hydrogen Energy* **2015**, *40*, 5916–5927. [CrossRef]
20. Hwang, S.H.; Kim, M.S. An Experimental Study on the Cathode Humidification and Evaporative Cooling of Polymer Electrolyte Membrane Fuel Cells Using Direct Water Injection Method at High Current Densities. *Appl. Therm. Eng.* **2016**, *99*, 635–644. [CrossRef]
21. Choi, E.J.; Hwang, S.H.; Park, J.; Kim, M.S. Parametric Analysis of Simultaneous Humidification and Cooling for PEMFCs Using Direct Water Injection Method. *Int. J. Hydrogen Energy* **2017**, *42*, 12531–12542. [CrossRef]
22. Konno, N.; Mizuno, S.; Nakaji, H.; Ishikawa, Y. Development of Compact and High-Performance Fuel Cell Stack. *SAE Int. J. Altern. Powertrains* **2015**, *4*, 123–129. [CrossRef]
23. Yoshizumi, T.; Kubo, H.; Okumura, M. *Development of High-Performance FC Stack for the New MIRAI*; SAE Technical Paper N°2021-01-740; SAE: Warrendale, PA, USA, 2021. [CrossRef]
24. Siegel, J.B.; McKay, D.A.; Stefanopoulou, A.G.; Hussey, D.S.; Jacobson, D.L. Measurement of Liquid Water Accumulation in a PEMFC with Dead-Ended Anode. *J. Electrochem. Soc.* **2008**, *155*, B1168. [CrossRef]
25. Meyer, Q.; Ashton, S.; Torija, S.; Gurney, C.; Boillat, P.; Cochet, M.; Engebretsen, E.; Finegan, D.P.; Adcock, P.; Shearing, P.R.; et al. Nitrogen Blanketing and Hydrogen Starvation in Dead-Ended-Anode Polymer Electrolyte Fuel Cells Revealed by Hydro-Electro-Thermal Analysis. *Electrochim. Acta* **2016**, *203*, 198–205. [CrossRef]
26. Asghari, S.; Ashraf Khorasani, M.R.; Dashti, I. Investigation of Self-Humidified and Dead-Ended Anode Proton Exchange Membrane Fuel Cell Performance Using Electrochemical Impedance Spectroscopy. *Int. J. Hydrogen Energy* **2016**, *41*, 12347–12357. [CrossRef]
27. Toghyani, S.; Baniasadi, E.; Afshari, E. Performance Analysis and Comparative Study of an Anodic Recirculation System Based on Electrochemical Pump in Proton Exchange Membrane Fuel Cell. *Int. J. Hydrogen Energy* **2018**, *43*, 19691–19703. [CrossRef]
28. Uno, M.; Shimada, T.; Tanaka, K. Reactant Recirculation System Utilizing Pressure Swing for Proton Exchange Membrane Fuel Cell. *J. Power Sources* **2011**, *196*, 2558–2566. [CrossRef]
29. Lee, H.-Y.; Su, H.-C.; Chen, Y.-S. A Gas Management Strategy for Anode Recirculation in a Proton Exchange Membrane Fuel Cell. *Int. J. Hydrogen Energy* **2018**, *43*, 3803–3808. [CrossRef]
30. Neyerlin, K.C.; Gasteiger, H.A.; Mittelsteadt, C.K.; Jorne, J.; Gu, W. Effect of Relative Humidity on Oxygen Reduction Kinetics in a PEMFC. *J. Electrochem. Soc.* **2005**, *152*, A1073. [CrossRef]
31. Yan, Q.; Toghiani, H.; Wu, J. Investigation of Water Transport through Membrane in a PEM Fuel Cell by Water Balance Experiments. *J. Power Sources* **2006**, *158*, 316–325. [CrossRef]
32. Lee, Y.; Kim, B.; Kim, Y. An Experimental Study on Water Transport through the Membrane of a PEFC Operating in the Dead-End Mode. *Int. J. Hydrogen Energy* **2009**, *34*, 7768–7779. [CrossRef]
33. Iranzo, A.; Boillat, P.; Biesdorf, J.; Salva, A. Investigation of the Liquid Water Distributions in a 50 Cm^2 PEM Fuel Cell: Effects of Reactants Relative Humidity, Current Density, and Cathode Stoichiometry. *Energy* **2015**, *82*, 914–921. [CrossRef]
34. Sanchez, D.G.; Ruiu, T.; Friedrich, K.A.; Sanchez-Monreal, J.; Vera, M. Analysis of the Influence of Temperature and Gas Humidity on the Performance Stability of Polymer Electrolyte Membrane Fuel Cells. *J. Electrochem. Soc.* **2016**, *163*, F150–F159. [CrossRef]
35. Sanchez, D.G.; Ruiu, T.; Biswas, I.; Schulze, M.; Helmly, S.; Friedrich, K.A. Local Impact of Humidification on Degradation in Polymer Electrolyte Fuel Cells. *J. Power Sources* **2017**, *352*, 42–55. [CrossRef]
36. Sanchez, D.G.; Garcia-Ybarra, P.L. PEMFC Operation Failure under Severe Dehydration. *Int. J. Hydrogen Energy* **2012**, *37*, 7279–7288. [CrossRef]

37. Gößling, S.; Klages, M.; Haußmann, J.; Beckhaus, P.; Messerschmidt, M.; Arlt, T.; Kardjilov, N.; Manke, I.; Scholta, J.; Heinzel, A. Analysis of Liquid Water Formation in Polymer Electrolyte Membrane (PEM) Fuel Cell Flow Fields with a Dry Cathode Supply. *J. Power Sources* **2016**, *306*, 658–665. [CrossRef]
38. De Bruijn, F.A.; Dam, V.A.T.; Janssen, G.J.M. Review: Durability and Degradation Issues of PEM Fuel Cell Components. *Fuel Cells* **2008**, *8*, 3–22. [CrossRef]
39. Wu, J.; Yuan, X.Z.; Martin, J.J.; Wang, H.; Zhang, J.; Shen, J.; Wu, S.; Merida, W. A Review of PEM Fuel Cell Durability: Degradation Mechanisms and Mitigation Strategies. *J. Power Sources* **2008**, *184*, 104–119. [CrossRef]
40. Yousfi-Steiner, N.; Moçotéguy, P.; Candusso, D.; Hissel, D.; Hernandez, A.; Aslanides, A. A Review on PEM Voltage Degradation Associated with Water Management: Impacts, Influent Factors and Characterization. *J. Power Sources* **2008**, *183*, 260–274. [CrossRef]
41. Werner, C.; Busemeyer, L.; Kallo, J. The Impact of Operating Parameters and System Architecture on the Water Management of a Multifunctional PEMFC System. *Int. J. Hydrogen Energy* **2015**, *40*, 11595–11603. [CrossRef]
42. Yakubu, A.U.; Zhao, J.; Jiang, Q.; Ye, X.; Liu, J.; Yu, Q.; Xiong, S. A Comprehensive Review of Primary Cooling Techniques and Thermal Management Strategies for Polymer Electrolyte Membrane Fuel Cells PEMFC. *Heliyon* **2024**, *10*, e38556. [CrossRef]
43. Yu, Y.; Chen, M.; Zaman, S.; Xing, S.; Wang, M.; Wang, H. Thermal Management System for Liquid-Cooling PEMFC Stack: From Primary Configuration to System Control Strategy. *eTransportation* **2022**, *12*, 100165. [CrossRef]
44. Bargal, M.H.S.; Abdelkareem, M.A.A.; Tao, Q.; Li, J.; Shi, J.; Wang, Y. Liquid Cooling Techniques in Proton Exchange Membrane Fuel Cell Stacks: A Detailed Survey. *Alex. Eng. J.* **2020**, *59*, 635–655. [CrossRef]
45. Cleghorn, S.J.C.; Derouin, C.R.; Wilson, M.S.; Gottesfeld, S. A Printed Circuit Board Approach to Measuring Current Distribution in a Fuel Cell. *J. Appl. Electrochem.* **1998**, *28*, 663–672. [CrossRef]
46. Stumper, J.; Campbell, S.A.; Wilkinson, D.P.; Johnson, M.C.; Davis, M. In-Situ Methods for the Determination of Current Distributions in PEM Fuel Cells. *Electrochimica Acta* **1998**, *43*, 3773–3783. [CrossRef]
47. Nguyen, T.V.; White, R.E. A Water and Heat Management Model for Proton-Exchange-Membrane Fuel Cells. *J. Electrochem. Soc.* **1993**, *140*, 2178–2186. [CrossRef]
48. Ji, M.; Wei, Z. A Review of Water Management in Polymer Electrolyte Membrane Fuel Cells. *Energies* **2009**, *2*, 1057–1106. [CrossRef]
49. Miao, T.; Tongsh, C.; Wang, J.; Cheng, P.; Liang, J.; Wang, Z.; Chen, W.; Zhang, C.; Xi, F.; Du, Q.; et al. Current Density and Temperature Distribution Measurement and Homogeneity Analysis for a Large-Area Proton Exchange Membrane Fuel Cell. *Energy* **2022**, *239*, 121922. [CrossRef]
50. Yan, S.; Yang, M.; Sun, C.; Xu, S. Liquid Water Characteristics in the Compressed Gradient Porosity Gas Diffusion Layer of Proton Exchange Membrane Fuel Cells Using the Lattice Boltzmann Method. *Energies* **2023**, *16*, 6010. [CrossRef]
51. Zhang, Y.; Tu, Z. Flow-Field Design of the Bipolar Plates in Polymer Electrolyte Membrane Fuel Cell: Problem, Progress, and Perspective. *Appl. Energy Combust. Sci.* **2024**, *17*, 100244. [CrossRef]
52. Abdullah, A.M.; Okajima, T.; Mohammad, A.M.; Kitamura, F.; Ohsaka, T. Temperature Gradients Measurements within a Segmented H2/Air PEM Fuel Cell. *J. Power Sources* **2007**, *172*, 209–214. [CrossRef]
53. Alaefour, I.; Karimi, G.; Jiao, K.; Li, X. Measurement of Current Distribution in a Proton Exchange Membrane Fuel Cell with Various Flow Arrangements—A Parametric Study. *Appl. Energy* **2012**, *93*, 80–89. [CrossRef]
54. Suárez, C.; Toharias, B.; Salva Aguirre, M.; Chesalkin, A.; Rosa, F.; Iranzo, A. Experimental Dynamic Load Cycling and Current Density Measurements of Different Inlet/Outlet Configurations of a Parallel-Serpentine PEMFC. *Energy* **2023**, *283*, 128455. [CrossRef]
55. Morin, A.; Balestrière, P.; LaManna, J.M.; Baltic, E.; Hussey, D.S.; Jacobson, D.L.; Vacquier, C.; Poirot-Crouvezier, J.-P. Experimental and Modeling Analyses of the Correlation between Local 3D Heterogeneities and the Macroscopic Observers of a Proton Exchange Membrane Fuel Cell Stack. *J. Electrochem. Soc.* **2024**, *171*, 044508. [CrossRef]
56. Dutta, S.S.S. Numerical Prediction of Temperature Distribution in Pem Fuel Cells. *Numer. Heat Transf. Part Appl.* **2000**, *38*, 111–128. [CrossRef]
57. Wang, M.; Guo, H.; Ma, C. Temperature Distribution on the MEA Surface of a PEMFC with Serpentine Channel Flow Bed. *J. Power Sources* **2006**, *157*, 181–187. [CrossRef]
58. Lee, C.-Y.; Hsieh, W.-J.; Wu, G.-W. Embedded Flexible Micro-Sensors in MEA for Measuring Temperature and Humidity in a Micro-Fuel Cell. *J. Power Sources* **2008**, *181*, 237–243. [CrossRef]
59. Lee, C.-Y.; Lee, S.-J.; Lo, Y.-M.; Liu, Y.-M. Micro Thermocouple and Voltage Sensor for Fuel Cell Real Time Interior Monitoring. *Int. J. Electrochem. Sci.* **2014**, *9*, 272–281. [CrossRef]
60. Pei, H.; Liu, Z.; Zhang, H.; Yu, Y.; Tu, Z.; Wan, Z.; Liu, W. In Situ Measurement of Temperature Distribution in Proton Exchange Membrane Fuel Cell I a Hydrogen–Air Stack. *J. Power Sources* **2013**, *227*, 72–79. [CrossRef]
61. Sundaresan, M.; Moore, R.M. Polymer Electrolyte Fuel Cell Stack Thermal Model to Evaluate Sub-Freezing Startup. *J. Power Sources* **2005**, *145*, 534–545. [CrossRef]

62. Liu, Z.; Mao, Z.; Wang, C.; Zhuge, W.; Zhang, Y. Numerical Simulation of a Mini PEMFC Stack. *J. Power Sources* **2006**, *160*, 1111–1121. [CrossRef]
63. Zhou, Y.; Luo, Y.; Yu, S.; Jiao, K. Modeling of Cold Start Processes and Performance Optimization for Proton Exchange Membrane Fuel Cell Stacks. *J. Power Sources* **2014**, *247*, 738–748. [CrossRef]
64. Macedo-Valencia, J.; Sierra, J.M.; Figueroa-Ramírez, S.J.; Díaz, S.E.; Meza, M. 3D CFD Modeling of a PEM Fuel Cell Stack. *Int. J. Hydrogen Energy* **2016**, *41*, 23425–23433. [CrossRef]
65. Fuller, T.F.; Newman, J. Water and Thermal Management in Solid-Polymer-Electrolyte Fuel Cells. *J. Electrochem. Soc.* **1993**, *140*, 1218–1225. [CrossRef]
66. Yan, Q.; Toghiani, H.; Causey, H. Steady State and Dynamic Performance of Proton Exchange Membrane Fuel Cells (PEMFCs) under Various Operating Conditions and Load Changes. *J. Power Sources* **2006**, *161*, 492–502. [CrossRef]
67. Nandjou, F.; Poirot-Crouvezier, J.-P.; Chandesris, M.; Blachot, J.-F.; Bonnaud, C.; Bultel, Y. Impact of Heat and Water Management on Proton Exchange Membrane Fuel Cells Degradation in Automotive Application. *J. Power Sources* **2016**, *326*, 182–192. [CrossRef]
68. Bao, C.; Ouyang, M.; Yi, B. Analysis of the Water and Thermal Management in Proton Exchange Membrane Fuel Cell Systems. *Int. J. Hydrogen Energy* **2006**, *31*, 1040–1057. [CrossRef]
69. Tardy, E.; Courtois, F.; Chandesris, M.; Poirot-Crouvezier, J.-P.; Morin, A.; Bultel, Y. Investigation of Liquid Water Heterogeneities in Large Area PEM Fuel Cells Using a Pseudo-3D Multiphysics Model. *Int. J. Heat Mass Transf.* **2019**, *145*, 118720. [CrossRef]
70. Huang, Y.; Xiao, X.; Kang, H.; Lv, J.; Zeng, R.; Shen, J. Thermal Management of Polymer Electrolyte Membrane Fuel Cells: A Critical Review of Heat Transfer Mechanisms, Cooling Approaches, and Advanced Cooling Techniques Analysis. *Energy Convers. Manag.* **2022**, *254*, 115221. [CrossRef]
71. Feng, B.; Lin, R.; Liu, D.; Zhong, D. Study on the Uncoupling Characteristics of PEM Fuel Cell by Segmented Cell Technology. *Int. J. Electrochem. Sci.* **2019**, *14*, 2175–2186. [CrossRef]
72. Fink, C.; Fouquet, N. Three-Dimensional Simulation of Polymer Electrolyte Membrane Fuel Cells with Experimental Validation. *Electrochim. Acta* **2011**, *56*, 10820–10831. [CrossRef]
73. Lobato, J.; Cañizares, P.; Rodrigo, M.A.; Pinar, F.J.; Mena, E.; Úbeda, D. Three-Dimensional Model of a 50 Cm2 High Temperature PEM Fuel Cell. Study of the Flow Channel Geometry Influence. *Int. J. Hydrogen Energy* **2010**, *35*, 5510–5520. [CrossRef]
74. Lobato, J.; Cañizares, P.; Rodrigo, M.A.; Pinar, F.J.; Úbeda, D. Study of Flow Channel Geometry Using Current Distribution Measurement in a High Temperature Polymer Electrolyte Membrane Fuel Cell. *J. Power Sources* **2011**, *196*, 4209–4217. [CrossRef]
75. Jabbour, L.; Robin, C.; Nandjou, F.; Vincent, R.; Micoud, F.; Poirot-Crouvezier, J.-P.; d'Arbigny, J.; Gerard, M. Feasibility of In-Plane GDL Structuration: Impact on Current Density Distribution in Large-Area Proton Exchange Membrane Fuel Cells. *J. Power Sources* **2015**, *299*, 380–390. [CrossRef]
76. Kraume, R. S++ Simulation Services. Available online: https://www.splusplus.com/measurement/en/csshunt.html (accessed on 12 November 2024).
77. Toharias, B.; Suárez, C.; Iranzo, A.; Salva, M.; Rosa, F. Dataset and Measurements from a Current Density Sensor during Experimental Testing of Dynamic Load Cycling for a Parallel-Serpentine Design of a Proton Exchange Membrane Fuel Cell. *Data Brief* **2024**, *54*, 110392. [CrossRef]
78. Chevalier, S.; Olivier, J.-C.; Josset, C.; Auvity, B. Polymer Electrolyte Membrane Fuel Cell Characterisation Based on Current Distribution Measurements. *ECS Trans.* **2018**, *86*, 211–220. [CrossRef]
79. Maranzana, G.; Lottin, O.; Colinart, T.; Chupin, S.; Didierjean, S. A Multi-Instrumented Polymer Exchange Membrane Fuel Cell: Observation of the in-Plane Non-Homogeneities. *J. Power Sources* **2008**, *180*, 748–754. [CrossRef]
80. Wieser, C.; Helmbold, A.; Gülzow, E. A New Technique for Two-Dimensional Current Distribution Measurements in Electrochemical Cells. *J. Appl. Electrochem.* **2000**, *30*, 803–807. [CrossRef]
81. Pérez, L.C.; Brandão, L.; Sousa, J.M.; Mendes, A. Segmented Polymer Electrolyte Membrane Fuel Cells—A Review. *Renew. Sustain. Energy Rev.* **2011**, *15*, 169–185. [CrossRef]
82. Trabold, T.A.; Owejan, J.P.; Gagliardo, J.J.; Jacobson, D.L.; Hussey, D.S.; Arif, M. Use of Neutron Imaging for Proton Exchange Membrane Fuel Cell (PEMFC) Performance Analysis and Design. In *Handbook of Fuel Cells*; Vielstich, W., Lamm, A., Gasteiger, H.A., Yokokawa, H., Eds.; Wiley: Hoboken, NJ, USA, 2010; ISBN 978-0-470-74151-1.
83. Hussey, D.S.; Jacobson, D.L.; Arif, M.; Coakley, K.J.; Vecchia, D.F. In Situ Fuel Cell Water Metrology at the NIST Neutron Imaging Facility. *J. Fuel Cell Sci. Technol.* **2010**, *7*, 021024. [CrossRef]
84. Jacobson, D.L.; Hussey, D.S.; Baltic, E. In Situ Imaging at the NIST Neutron Imaging Facility. *MRS Proc.* **2011**, *1318*, mrsf10-1318-ss02-01. [CrossRef]
85. Alink, R.; Gerteisen, D. Coupling of a Continuum Fuel Cell Model with a Discrete Liquid Water Percolation Model. *Int. J. Hydrogen Energy* **2014**, *39*, 8457–8473. [CrossRef]
86. García-Salaberri, P.A.; Sánchez, D.G.; Boillat, P.; Vera, M.; Friedrich, K.A. Hydration and Dehydration Cycles in Polymer Electrolyte Fuel Cells Operated with Wet Anode and Dry Cathode Feed: A Neutron Imaging and Modeling Study. *J. Power Sources* **2017**, *359*, 634–655. [CrossRef]

87. Basu, S.; Renfro, M.W.; Cetegen, B.M. Spatially Resolved Optical Measurements of Water Partial Pressure and Temperature in a PEM Fuel Cell under Dynamic Operating Conditions. *J. Power Sources* **2006**, *162*, 286–293. [CrossRef]
88. Basu, S.; Renfro, M.W.; Gorgun, H.; Cetegen, B.M. In Situ Simultaneous Measurements of Temperature and Water Partial Pressure in a PEM Fuel Cell under Steady State and Dynamic Cycling. *J. Power Sources* **2006**, *159*, 987–994. [CrossRef]
89. Brett, D.J.L.; Atkins, S.; Brandon, N.P.; Vasileiadis, N.; Vesovic, V.; Kucernak, A.R. Membrane Resistance and Current Distribution Measurements under Various Operating Conditions in a Polymer Electrolyte Fuel Cell. *J. Power Sources* **2007**, *172*, 2–13. [CrossRef]
90. Yu, W.; Sun, L.; Zhu, W.; Li, Y.; Pei, H.; Xing, L. Investigation of Non-Uniform Temperature Distribution in Air-Cooled Proton Exchange Membrane Fuel Cells with Multizone Temperature Measurement. *Int. J. Green Energy* **2024**, *21*, 2228–2238. [CrossRef]
91. Zhang, Y.; He, S.; Jiang, X.; Yang, X.; Wang, Z.; Zhang, S.; Cao, J.; Fang, H.; Li, Q. Full-Scale Three-Dimensional Simulation of Air Cooling Metal Bipolar Plate Proton Exchange Membrane Fuel Cell Stack Considering a Non-Isothermal Multiphase Model. *Appl. Energy* **2024**, *357*, 122507. [CrossRef]
92. Jiang, H.; Wang, X.; Ding, C.; Shan, D.; Guo, B.; Qi, H.; Xu, J. A Review of Emerging Design and Theoretical Progress on Vapor Chamber for Efficient Thermal Performance. *Int. J. Heat Mass Transf.* **2024**, *231*, 125814. [CrossRef]
93. Zhao, J.; Jian, Q.; Huang, Z. Experimental Study on Heat Transfer Performance of Vapor Chambers with Potential Applications in Thermal Management of Proton Exchange Membrane Fuel Cells. *Appl. Therm. Eng.* **2020**, *180*, 115847. [CrossRef]
94. Choi, J.; Kim, Y.-H.; Lee, Y.; Lee, K.-J.; Kim, Y. Numerical Analysis on the Performance of Cooling Plates in a PEFC. *J. Mech. Sci. Technol.* **2008**, *22*, 1417–1425. [CrossRef]
95. Yu, S.H.; Sohn, S.; Nam, J.H.; Kim, C.-J. Numerical Study to Examine the Performance of Multi-Pass Serpentine Flow-Fields for Cooling Plates in Polymer Electrolyte Membrane Fuel Cells. *J. Power Sources* **2009**, *194*, 697–703. [CrossRef]
96. Afshari, E.; Ziaei-Rad, M.; Shariati, Z. A Study on Using Metal Foam as Coolant Fluid Distributor in the Polymer Electrolyte Membrane Fuel Cell. *Int. J. Hydrogen Energy* **2016**, *41*, 1902–1912. [CrossRef]
97. Ghasemi, M.; Ramiar, A.; Ranjbar, A.A.; Rahgoshay, S.M. A Numerical Study on Thermal Analysis and Cooling Flow Fields Effect on PEMFC Performance. *Int. J. Hydrogen Energy* **2017**, *42*, 24319–24337. [CrossRef]
98. Vazifeshenas, Y.; Sedighi, K.; Shakeri, M. Heat Transfer in PEM Cooling Flow Field with High Porosity Metal Foam Insert. *Appl. Therm. Eng.* **2019**, *147*, 81–89. [CrossRef]
99. Li, S.; Ake Sunden, B. Numerical Analysis on Thermal Performance of Cooling Plates with Wavy Channels in PEM Fuel Cells. *Int. J. Numer. Methods Heat Fluid Flow* **2018**, *28*, 1684–1697. [CrossRef]
100. Chen, X.; Liu, Q.; Fang, Y.; He, L.; Huang, T.; Zhang, Y.; Wan, Z.; Wang, X. Numerical Study of a MIMO-Shaped Cooling Plate in PEMFC Stack for Heat Transfer Enhancement. *Energy Rep.* **2021**, *7*, 5804–5814. [CrossRef]
101. Kai, Y.; Kitayama, Y.; Omiya, M.; Uchiyama, T.; Kato, M. Crack Formation in Membrane Electrode Assembly Under Static and Cyclic Loadings. *J. Fuel Cell Sci. Technol.* **2013**, *10*, 21007. [CrossRef]
102. Zhang, Z.; Mao, J.; Liu, Z. Advancements and Insights in Thermal and Water Management of Proton Exchange Membrane Fuel Cells: Challenges and Prospects. *Int. Commun. Heat Mass Transf.* **2024**, *153*, 107376. [CrossRef]
103. Costamagna, P.; Srinivasan, S. Quantum Jumps in the PEMFC Science and Technology from the 1960s to the Year 2000: Part II. Engineering, Technology Development and Application Aspects. *J. Power Sources* **2001**, *102*, 253–269. [CrossRef]
104. Li, X.; Sabir, I. Review of Bipolar Plates in PEM Fuel Cells: Flow-Field Designs. *Int. J. Hydrogen Energy* **2005**, *30*, 359–371. [CrossRef]
105. Chen, F.C.; Gao, Z.; Loutfy, R.O.; Hecht, M. Analysis of Optimal Heat Transfer in a PEM Fuel Cell Cooling Plate. *Fuel Cells* **2003**, *3*, 181–188. [CrossRef]
106. Atyabi, S.A.; Afshari, E.; Zohravi, E.; Udemu, C.M. Three-Dimensional Simulation of Different Flow Fields of Proton Exchange Membrane Fuel Cell Using a Multi-Phase Coupled Model with Cooling Channel. *Energy* **2021**, *234*, 121247. [CrossRef]
107. Miri Joibary, S.M.; Rahgoshay, S.M.; Rahimi-Esbo, M.; Firouzjaee, K.D. Numerical Investigation of the Influence of Different Cooling Flow Channels on the Thermal and Water Saturation Distribution in a Real Dimensional Polymer Electrolyte Membrane Fuel Cell. *Int. J. Hydrogen Energy* **2023**, *48*, 2762–2787. [CrossRef]
108. Zhang, Z.; Li, Z.; Lin, W.; Chen, J.; Tao, W. Effect of Cooling Flow Channels on the In-Plane Temperature Distribution in PEMFC. In *Advances in Computational Heat and Mass Transfer*; Benim, A.C., Bennacer, R., Mohamad, A.A., Ocłoń, P., Suh, S.-H., Taler, J., Eds.; Lecture Notes in Mechanical Engineering; Springer International Publishing: Cham, Switzerland, 2024; pp. 644–654, ISBN 978-3-031-67240-8.
109. Xu, X.; Zhang, L.; Wang, S.; Han, D.; You, S.; Zhou, J. Numerical and Experimental Analyses of a Novel Type PEMFC Coolant Channel. *Int. J. Hydrogen Energy* **2024**, *49*, 652–673. [CrossRef]
110. Baek, S.M.; Yu, S.H.; Nam, J.H.; Kim, C.-J. A Numerical Study on Uniform Cooling of Large-Scale PEMFCs with Different Coolant Flow Field Designs. *Appl. Therm. Eng.* **2011**, *31*, 1427–1434. [CrossRef]
111. Sasmito, A.P.; Kurnia, J.C.; Mujumdar, A.S. Numerical Evaluation of Various Gas and Coolant Channel Designs for High Performance Liquid-Cooled Proton Exchange Membrane Fuel Cell Stacks. *Energy* **2012**, *44*, 278–291. [CrossRef]

112. Ravishankar, S.; Arul Prakash, K. Numerical Studies on Thermal Performance of Novel Cooling Plate Designs in Polymer Electrolyte Membrane Fuel Cell Stacks. *Appl. Therm. Eng.* **2014**, *66*, 239–251. [CrossRef]
113. Rahgoshay, S.M.; Ranjbar, A.A.; Ramiar, A.; Alizadeh, E. Thermal Investigation of a PEM Fuel Cell with Cooling Flow Field. *Energy* **2017**, *134*, 61–73. [CrossRef]
114. Song, J.; Huang, Y.; Zeng, J.; Chen, L.; Wu, Y. Design and Numerical Investigation of Multi-Channel Cooling Plate for Proton Exchange Membrane Fuel Cell. *Energy Rep.* **2022**, *8*, 6058–6067. [CrossRef]
115. Liu, X.; Bai, M.; Zhou, Z.; Poramapojana, P.; Li, Y.; Gao, L.; Li, Y.; Song, Y. Three-Dimensional Multi-Phase Numerical Study for the Effect of Coolant Flow Field Designs on Water and Thermal Management for the Large-Scale PEMFCs. *Int. J. Hydrogen Energy* **2023**, *48*, 23681–23705. [CrossRef]
116. Huo, W.; Liu, B.; Xu, W.; Xie, B.; Fan, L.; Benbouzid, M.; Xu, Y.; Ding, T.; Fang, C.; Gao, F.; et al. High Precision and Efficient Simulation of Large-Size Proton Exchange Membrane Fuel Cells Incorporated with a Novel Alternative Cooling Method. *Int. J. Heat Mass Transf.* **2024**, *230*, 125780. [CrossRef]
117. Chen, Y.; Jiang, X.; Zhang, Y.; Gu, M.; Xiong, K.; Liu, L. Investigation of Heat and Mass Transfer Properties of the Wave Staggered Round Table Cooling Flow Field with a Three-Stage Forked Distribution Zone. *J. Power Sources* **2024**, *623*, 235484. [CrossRef]
118. Chen, B.; Deng, Q.; Yang, G.; Zhou, Y.; Chen, W.; Cai, Y.; Tu, Z. Numerical Study on Heat Transfer Characteristics and Performance Evaluation of PEMFC Based on Multiphase Electrochemical Model Coupled with Cooling Channel. *Energy* **2023**, *285*, 128933. [CrossRef]
119. Zhu, K.-Q.; Ding, Q.; Zhang, B.-X.; Xu, J.-H.; Yang, Y.-R.; Lee, D.-J.; Wan, Z.-M.; Wang, X.-D. Evaluation of Performance and Mass Transfer Characteristics by Applying Oblique Fin Flow Field to Air-Cooled PEMFCs under Different Ambient Conditions. *Sustain. Energy Technol. Assess.* **2023**, *60*, 103517. [CrossRef]
120. Zhu, K.-Q.; Ding, Q.; Zhang, B.-X.; Xu, J.-H.; Li, D.-D.; Yang, Y.-R.; Lee, D.-J.; Wan, Z.-M.; Wang, X.-D. Performance Enhancement of Air-Cooled PEMFC Stack by Employing Tapered Oblique Fin Channels: Experimental Study of a Full Stack and Numerical Analysis of a Typical Single Cell. *Appl. Energy* **2024**, *358*, 122595. [CrossRef]
121. Chen, X.; Chai, F.; Hu, S.; Tan, J.; Luo, L.; Xie, H.; Wan, Z.; Qu, Z. Design of PEMFC Bipolar Plate Cooling Flow Field Based on Fractal Theory. *Energy Convers. Manag. X* **2023**, *20*, 100445. [CrossRef]
122. Liu, Y.; Zeng, L.; Chen, Y.; Zhang, X. Improving the Cooling Effect of Proton Exchange Membrane Fuel Cells by Using Biomimetic Capillary Cooling Channels Based on Topology Optimization Method. *Appl. Therm. Eng.* **2024**, *251*, 123633. [CrossRef]
123. Zhang, X.; Huang, Y.; Ma, Z.; Gao, T. Study on Heat Transfer Enhancement Performance of Cooling Channel with Elliptical Dimples in a Proton Exchange Membrane Fuel Cell. *Int. Commun. Heat Mass Transf.* **2024**, *153*, 107343. [CrossRef]
124. Poirot-Crouvezier, J.-P.; Roy, F. GENEPAC Project: Realization of a fuel cell stack prototype dedicated to the automotive application. In Proceedings of the 16th World Hydrogen Energy Conference 2006, WHEC 2006, Lyon, France, 13–16 June 2006; pp. 2820–2824.
125. Nandjou, F.; Poirot-Crouvezier, J.-P.; Chandesris, M.; Bultel, Y. A Pseudo-3D Model to Investigate Heat and Water Transport in Large Area PEM Fuel Cells—Part 1: Model Development and Validation. *Int. J. Hydrogen Energy* **2016**, *41*, 15545–15561. [CrossRef]
126. Mahdavi, A.; Ranjbar, A.A.; Gorji, M.; Rahimi-Esbo, M. Numerical Simulation Based Design for an Innovative PEMFC Cooling Flow Field with Metallic Bipolar Plates. *Appl. Energy* **2018**, *228*, 656–666. [CrossRef]
127. Rahimi-Esbo, M.; Rahgoshay, S.M.; Hassani, M.M.; Dadashi Firouzjaei, K. Novel Design and Numerical Evaluating of a Cooling Flow Field in PEMFC with Metallic Bipolar Plates. *Int. J. Hydrogen Energy*, 2020; *in press*. [CrossRef]
128. Xu, P.; Zhu, J.; Xu, L.; Zhang, X.; Qiu, S.; Gu, H.; Mujumdar, A.S. Bionic Tree-like Microchannel with Steady and Pulsating Flow for Thermal Management of Proton Exchange Membrane Fuel Cell. *Int. J. Hydrogen Energy* **2024**, *93*, 328–337. [CrossRef]
129. Nandjou, F.; Poirot-Crouvezier, J.-P.; Chandesris, M.; Rosini, S.; Hussey, D.S.; Jacobson, D.L.; LaManna, J.M.; Morin, A.; Bultel, Y. A Pseudo-3D Model to Investigate Heat and Water Transport in Large Area PEM Fuel Cells—Part 2: Application on an Automotive Driving Cycle. *Int. J. Hydrogen Energy* **2016**, *41*, 15573–15584. [CrossRef]
130. Shen, H.; Huang, Y.; Kang, H.; Shen, J.; Yu, J.; Zhang, J.; Li, Z. Effect of the Cooling Water Flow Direction on the Performance of PEMFCs. *Int. J. Heat Mass Transf.* **2022**, *189*, 122303. [CrossRef]
131. Zhang, G.; Xie, X.; Xie, B.; Du, Q.; Jiao, K. Large-Scale Multi-Phase Simulation of Proton Exchange Membrane Fuel Cell. *Int. J. Heat Mass Transf.* **2019**, *130*, 555–563. [CrossRef]
132. Amirfazli, A.; Asghari, S.; Koosha, M. Mathematical Modeling and Simulation of Thermal Management in Polymer Electrolyte Membrane Fuel Cell Stacks. *J. Power Sources* **2014**, *268*, 533–545. [CrossRef]
133. Cornet, M.; Poirot-Crouvezier, J.-P.; Schott, P.; Kawka, S.; Morin, A.; Bultel, Y. Advanced Methodology for Simulating Local Operating Conditions in Large Fuel Cells Based on a Spatially Averaged Pseudo-3D Model. *J. Electrochem. Soc.* **2024**, *171*, 104514. [CrossRef]
134. Schmittinger, W.; Vahidi, A. A Review of the Main Parameters Influencing Long-Term Performance and Durability of PEM Fuel Cells. *J. Power Sources* **2008**, *180*, 1–14. [CrossRef]

135. Pei, P.; Chen, H. Main Factors Affecting the Lifetime of Proton Exchange Membrane Fuel Cells in Vehicle Applications: A Review. *Appl. Energy* **2014**, *125*, 60–75. [CrossRef]
136. Durst, J.; Lamibrac, A.; Charlot, F.; Dillet, J.; Castanheira, L.F.; Maranzana, G.; Dubau, L.; Maillard, F.; Chatenet, M.; Lottin, O. Degradation Heterogeneities Induced by Repetitive Start/Stop Events in Proton Exchange Membrane Fuel Cell: Inlet vs. Outlet and Channel vs. Land. *Appl. Catal. B Environ.* **2013**, *138–139*, 416–426. [CrossRef]
137. Gazdzicki, P.; Mitzel, J.; Sanchez, D.G.; Aßmann, P.; Sousa, J.; Morawietz, T.; Hiesgen, R.; Häußler, F.; Hunger, J.; Schlumberger, G.; et al. Operando and Ex-Situ Investigation of PEMFC Degradation. *ECS Trans.* **2019**, *92*, 261–276. [CrossRef]
138. Lochner, T.; Hallitzky, L.; Perchthaler, M.; Obermaier, M.; Sabawa, J.; Enz, S.; Bandarenka, A.S. Local Degradation Effects in Automotive Size Membrane Electrode Assemblies under Realistic Operating Conditions. *Appl. Energy* **2020**, *260*, 114291. [CrossRef]
139. Garcia-Sanchez, D.; Morawietz, T.; Da Rocha, P.G.; Hiesgen, R.; Gazdzicki, P.; Friedrich, K.A. Local Impact of Load Cycling on Degradation in Polymer Electrolyte Fuel Cells. *Appl. Energy* **2020**, *259*, 114210. [CrossRef]
140. Rodosik, S.; Poirot-Crouvezier, J.-P.; Bultel, Y. Impact of Alternating Fuel Feeding on a PEMFC Stack Durability. *Int. J. Hydrogen Energy* **2021**, *46*, 39415–39426. [CrossRef]
141. Bultel, Y.; Bas, C.; Dubelley, F.; Micoud, F.; Nayoze-Coynel, C.; Rosini, S. Anode Defects' Propagation in Polymer Electrolyte Membrane Fuel Cells Stack. *Int. J. Hydrogen Energy* **2024**, *82*, 257–264. [CrossRef]
142. Borup, R.L.; Mukundan, R. PEM Fuel Cell Degradation. *ECS Trans.* **2010**, *33*, 17–26. [CrossRef]
143. Ren, P.; Pei, P.; Li, Y.; Wu, Z.; Chen, D.; Huang, S. Degradation Mechanisms of Proton Exchange Membrane Fuel Cell under Typical Automotive Operating Conditions. *Prog. Energy Combust. Sci.* **2020**, *80*, 100859. [CrossRef]
144. Koprek, M.; Schlumberger, R.; Wachtel, C.; Wilhelm, F.; Messerschmidt, M.; Scholta, J.; Hölzle, M. Local Ageing Effects of Polymer Electrolyte Fuel Cell Membrane Electrode Assemblies Due to Accelerated Durability Testing. *Fuel Cells* **2022**, *22*, 271–283. [CrossRef]
145. Meng, X.; Sun, C.; Mei, J.; Tang, X.; Hasanien, H.M.; Jiang, J.; Fan, F.; Song, K. Fuel Cell Life Prediction Considering the Recovery Phenomenon of Reversible Voltage Loss. *J. Power Sources* **2025**, *625*, 235634. [CrossRef]
146. Gerard, M.; Poirot-Crouvezier, J.-P.; Hissel, D.; Péra, M.-C. Ripple Current Effects on PEMFC Aging Test by Experimental and Modeling. *J. Fuel Cell Sci. Technol.* **2011**, *8*, 021004. [CrossRef]
147. Gerard, M.; Poirot-Crouvezier, J.-P.; Hissel, D.; Pera, M.-C. Distribution Study of Species and Current Density During Oxygen Starvation. *J. Fuel Cell Sci. Technol.* **2010**, *7*, 51010. [CrossRef]
148. Drugeot, T.; Micoud, F.; Pinton, E.; Rosini, S.; Poirot-Crouvezier, J.-P.; Poupin, L.; Bultel, Y. Experimental Assessment of Proton Exchange Membrane Fuel Cell Performance Degradations during Emulated Start-up/Shut-down Phases. *Int. J. Hydrogen Energy* **2023**, *48*, 5630–5642. [CrossRef]
149. Drugeot, T.; Wane, R.; Micoud, F.; Pinton, E.; Guetaz, L.; Mermoux, M.; Bultel, Y. Cathode Catalyst Layer Aging of Proton Exchange Membrane Fuel Cell during Emulated Start-up/Shut-down Phases. *Int. J. Hydrogen Energy* **2024**, *87*, 838–847. [CrossRef]
150. Lai, Y.-H.; Fly, G.W. In-Situ Diagnostics and Degradation Mapping of a Mixed-Mode Accelerated Stress Test for Proton Exchange Membranes. *J. Power Sources* **2015**, *274*, 1162–1172. [CrossRef]
151. Lochner, T.; Kluge, R.M.; Fichtner, J.; El-Sayed, H.A.; Garlyyev, B.; Bandarenka, A.S. Temperature Effects in Polymer Electrolyte Membrane Fuel Cells. *ChemElectroChem* **2020**, *7*, 3545–3568. [CrossRef]
152. Chandesris, M.; Guetaz, L.; Schott, P.; Scohy, M.; Escribano, S. Investigation of Degradation Heterogeneities in PEMFC Stack Aged under Reformate Coupling In Situ Diagnosis, Post-Mortem Ex Situ Analyses and Multi-Physic Simulations. *J. Electrochem. Soc.* **2018**, *165*, F3290–F3306. [CrossRef]
153. Pauchet, J.; Prat, M.; Schott, P.; Kuttanikkad, S.P. Performance Loss of Proton Exchange Membrane Fuel Cell Due to Hydrophobicity Loss in Gas Diffusion Layer: Analysis by Multiscale Approach Combining Pore Network and Performance Modelling. *Int. J. Hydrogen Energy* **2012**, *37*, 1628–1641. [CrossRef]
154. European Commission: Joint Research Centre; De Marco, G.; Malkow, T.; Tsotridis, G.; Pilenga, A. EU Harmonised Test Protocols for PEMFC MEA Testing in Single Cell Configuration for Automotive Applications, Publications Office. 2015. Available online: https://data.europa.eu/doi/10.2790/54653 (accessed on 18 November 2024).
155. Collier, A.; Wang, H.; Ziyuan, X.; Zhang, J.; Wilkinson, D. Degradation of Polymer Electrolyte Membranes. *Int. J. Hydrogen Energy* **2006**, *31*, 1838–1854. [CrossRef]
156. Nandjou, F. Local Thermal Analysis of Fuels Cells for Automotive Application. Impact on Durability. Ph.D. Dissertation, University of Grenoble Alpes, Grenoble, France, 2015. Available online: https://theses.hal.science/tel-01267255/ (accessed on 18 November 2024).